SKYLAB FLOATING ICE EXPERIMENT - FINAL REPORT

by

W.J. Campbell, P. I. eng
U.S. Geological Survey, University of Puget Sound
Tacoma, Washington 98416

R.O. Ramseier and R.J. Weaver
Department of the Environment
580 Booth Street
Ottawa, Ontario K1A 0H3

W.F. Weeks
U.S. Army Cold Regions Research and Engineering Laboratory
Hanover, New Hampshire 13755

prepared for

NATIONAL AERONAUTICS AND SPACE ADMINISTRATION
SCIENCE AND APPLICATIONS DIRECTORATE
LYNDON B. JOHNSON SPACE CENTER
HOUSTON, TEXAS 77058

December, 1975

1. INTRODUCTION

The following report describes the only SKYLAB experiment concerned with either lake ice or sea ice. The specific areas of study are of scientific and economic interest to both Canada and the United States inasmuch as they comprise part of the waters of the shipping route between the Atlantic Ocean and the Great Lakes.

Earlier remote sensing studies of sea ice (Campbell et al, 1974, Ramseier et al, 1974) revealed that detailed surface truth and aircraft observations were necessary in order to properly interpret satellite photography and imagery, especially in the microwave region. Therefore, in the initial design of this experiment we planned a comprehensive surface and aircraft program to occur in close simultaneity with Skylab-4 overpasses of selected test sites. The accomplishment of this plan was difficult. No one government, let alone one agency, could put at our disposal all the aircraft, ship, and hovercraft support needed for the ground truth programs. It was only by obtaining the support of a large number of individuals and agencies that we were able to proceed. The time-consuming process of arranging all this was greatly complicated by 1) the possibility that the Skylab-4 flight would end in both test areas before the onset of the ice seasons (it almost did due to the gyroscope failures); 2) the fact that we could not know in advance the days on which the Skylab sensors would be turned on over our test areas; 3) the fact that the remote sensing aircraft available to us had only limited time periods free for our use; 4) the fact that our experiment occurred during the season of most inclement weather in both test areas; and 5) the fact that our test areas were geographically extensive.

In the following we present a spacecraft-aircraft-surface multi-sensor view of sea ice in the Gulf of St. Lawrence and lake ice in the Thousand Islands-St. Lawrence River during January-February 1974. The ensemble of data is complex, including imagery and photography from Skylab-4 (SL-4); the Argus remote sensing aircraft of the Canadian Forces Maritime Proving and Evaluation Unit operating from Summerside, Prince Edward Island; the NASA NP-3A remote sensing aircraft operating from the Johnson Space Center, Houston; a Canadian Coast Guard helicopter operating from Prescott, Ontario; three hovercraft of the Canadian Department of the Environment operating from Wolfe Island, Thousand Islands; and the Canadian oceanographic vessel CSS Dawson operating from the Bedford Institute of Oceanography, Dartmouth, Nova Scotia. Due to the wide variety of sensor platforms that were used and the rather extreme environmental constraints that were encountered and which affected different sensors in different ways, we were not always able to accomplish near-simultaneity of data sets in the three-level observing system. However, we believe that the data collected gives a new view of the ice in these regions which we hope will serve as an aid to image interpretation of similar ice in other areas (Bering

Sea, Baltic Sea, Sea of Okhotsk, Great Lakes, Lake Baikal) at the normal times when such multi-level, multi-sensor data are not available.

2. GULF OF ST. LAWRENCE

2.1 Description of Experiment

Skylab-4 Earth Resources Experiment Program (EREP) passes of the Gulf were made on 11, 12, 14, and 23 January 1974. The paths of these passes and orbit numbers are shown in Figure 1. Hand-held camera shots of the Gulf were made by the SL-4 astronauts whenever cloud conditions permitted. These photographs have been discussed in detail in Campbell et al (1975), which is part of the Skylab Visual Observations Report. Some of these photographs are necessary for this report and are shown as Figures 3-12, which includes one photograph obtained on 11 January 1974, two on 18 January, one on 19 January, four on 20 January, and one on 21 January.

The Argus aircraft conducted side-looking airborne radar (SLAR) and infrared runs over portions of the Gulf on 13 and 18 January 1974. The tracks of these flights are shown in Figure 1. The NASA NP-3A aircraft also flew over the Gulf on 16 and 21 January (the tracks of which are also shown in Figure 1). The key sensors used on these specific flights were the passive microwave imaging system (PMIS), the infrared scanner, the multifrequency microwave radiometer (MFMR), and two RC-8 cameras.

In addition the CSS Dawson operated in the ice-covered portions of the Gulf between 8 and 15 January 1974, when operations in the ice pack had to be terminated because of a compressor malfunction. Therefore, the only aircraft flight for which simultaneous ground truth was obtained was that of the Argus on 13 January 1974. Fortunately, the Dawson was in the Gulf during the first three Skylab EREP passes. Numerous ice photographs and ice salinity and temperature measurements were obtained by the ground truth team onboard the Dawson (Dunbar and Weeks, 1975) and four photographs of ice forms observed during its transit are shown in Figure 2. The track of the Dawson is also shown in Figure 1.

2.2 Ice Regime

The Gulf of St. Lawrence develops an ice cover in the winter only, with the growth of the pack normally running from December to March, when melting starts. The ice has usually completely disappeared by early May. Thus the ice never develops beyond the first-year stage with its maximum undeformed thickness being in the range of 75 to 90 cm. The Gulf in winter is an extremely active area both meteorologically and oceanographically. Frequent intense cyclonic passages coupled with strong geostrophic and tidal currents result in a fast moving pack which undergoes major deformation. The Skylab visual

observation data provide excellent synoptic information on the rapidly varying ice conditions which existed during the experiment.

The first useful photograph was taken on January 6 (Figure 3). It clearly shows a number of ice features characteristic of the early ice growth period on the Gulf. The heaviest ice conditions are found in the western part of the Gulf and even there the pack is quite open. The heaviest ice appears to be grey-white ice (the reader can find a glossary of ice terms at the rear of this document) which is particularly abundant along the south-western side of the Gulf. As one moves toward the north shore, grey ice becomes the predominant ice type with an open lead usually persisting along the north coast. This ice thickness distribution reflects the general ice drift pattern to the south and east into the central Gulf. Also of note are indications of pronounced ice divergence during this drift resulting in up to 25% open water. The only ice visible near Anticosti Island are some ice plumes off its southwest coast. Note also that the fast ice in the bays on the eastern part of the Gaspe Peninsula is only partially developed.

Two surface photographs taken from the CSS Dawson of the two principal ice types present at this time are shown in Figures 2a and 2b. The first of these figures shows a field of consolidated pancake ice just east of the eastern tip of the Gaspe Peninsula and the second figure shows typical newly-formed grey-white ice near the north shore. Pressure ridging associated with differential ice motion was quite common in the heavier ice (Figure 2c).

Figure 4 shows the ice distribution in the vicinity of the northeastern portion of the Gulf on January 11 as viewed from Skylab. At this time there is still only lightly developed ice present to the southwest of the Straits of Belle Isle. Note that the thickest ice occurs just to the southwest of the neck of the Strait. The most striking features on this photograph are the ice plumes that occur to the east of Newfoundland and Labrador. Figures 2d and 2e show an aircraft and a surface view of these types of plumes. The ice here is unconsolidated frazil which is kept from congealing into a continuous solid ice cover by the continuous passage of waves through the plumes. These features appear to characteristically form at the edge of the pack during periods of high winds. These plumes can best be described as possessing a vortex type of structure. Note in Figure 4 the vortex lines flowing around Belle Isle and the Grey Islands located further to the south. The small plumes that are composed of slush are elongated parallel to the surface wind (also verified by shipboard observations).

The next cloud-free SL-4 photograph of this area was taken on January 19. The most striking feature on this photograph (Figure 5) is the strongly developed plume structure off Newfoundland. Note the marked difference in the structure of

these plumes compared to the ones discussed earlier in that these plumes are now elongated perpendicular to the surface wind direction as deduced from the stratocumulus bands. We suggest that while the earlier plumes were composed of slush, this orientation change indicates that these present plumes are composed of deformed pack ice. The presence of open water and grey ice in the lee of Newfoundland and the Belle and Grey Islands is due to the combined effects of the offshore surface winds and the southerly flowing surface currents.

Figure 6, obtained a day later, shows the further development of the area of thicker ice just west of the Straits of Belle Isle that was referred to in Figure 4. Considering the open water along the Quebec shore and the fracture pattern of the leads, it appears that the ice in the northeastern Gulf has recently been advected towards the southwest. Note that the ice in the western part of the Straits appears to be thinner. This also can clearly be seen in Figure 7 taken later on the same orbit. These observations suggest that there was no pronounced flux of ice northeastwards through the Straits of Belle Isle. The fact that the zone of heavier ice remains relatively static at the southwest end of the Straits also suggests that there was no strong flux of ice at this time from the Labrador Sea through the Strait into the Gulf.

Figures 8 and 9 show the ice patterns in the general area of the Gaspe Peninsula in 18 and 20 January respectively. These two photographs show the most rapid period of ice growth observed in this experiment. Note the dramatic increase in ice thickness in the Baie des Chaleurs. Also note the heavier ice that has been advected through the Gaspe Passage into the area to the east of the Gaspe Peninsula. These photographs also show a large open lead along the north bank of the St. Lawrence River. This feature was quite common in other SL-4 photography. The fairly constant southerly surface winds during this period advected the ice away from the coast causing this zone to be one of strong ice production. In this time period between these figures and Figure 3 (6 January to 20 January) there had also been extensive fast ice development in the Baie de Gaspe.

The behaviour of the ice in the vicinity of Anticosti Island on 18 and 20 January is clearly shown in Figures 10 and 11. As was observed further to the west, the interval between these photographs was a time of pronounced ice growth. Again note the presence of the shore lead-along the entire north shore of the Gulf extending as far east as the heavy ice zone at the neck of the Strait of Belle Isle (see also Figure 7). Therefore, during this period the entire northern edge of the Gulf served as a source area for ice which was then advected to the south. The lead patterns in Figure 11 are quite interesting in that they show a generally extending flow in ice into the Southern Gulf except in the Jacques Cartier Passage where this flow is blocked by Anticosti Island. This blockage results in north-south leads produced by the local compressional flow resulting in lateral

divergence to the east and the west. Note also the chevron pattern in the lead structure to the northeast of Anticosti. Again this results from the blocking effect of the island.

Perhaps the most striking ice feature in the vicinity of Anticosti Island is the vortex structure that forms in the lee (to the south) of the island. The development of the vortex pattern can be seen in Figures 10, 11, and 12, in which a fairly unperturbed flow of ice progressed into one with large perturbations (order of 150 Km) in the period of three days. During the three weeks of the Skylab Gulf experiment, this vortex feature was continuously developed, and this area was one of constant ice production. Finally, note in Figure 7 the beautiful example of the development of stratoculumus plumes as the cold surface air flows from the ice over the open water area in the vicinity of Cabot Strait. The manner in which the entire pack rapidly adjusts to changes in wind direction can also clearly be seen in Figures 7 and 12. The southerly surface winds acting on the pack in 20 January changed to easterly during the night, partially closing the shore lead along the Jacques Cartier Passage.

A series of four ice reconnaissance maps for the period 8-22 January 1974 prepared by Ice Centrel, Department of the Environment, Canada, is shown in Figures 13 through 16. These maps were prepared using both aircraft and satellite data.

The above photographs and maps illustrate the dynamic and complex nature of the St. Lawrence ice cover. It's behaviour during this experiment was similar to that of preceeding years with the exception that the pack on the average was slightly thicker than normal for the time of year. The large spatial variations of the pack that occur at small times scales make it a phenomenon whose ultimate cause and effect can be understood only with the aid of remote sensing techniques.

2.3 Skylab Observations

This experiment emphasized the remote sensing of ice by both passive and active microwave techniques. This thrust dominated the design of the experiment from the start for several reasons. First, because floating ice is commonly obscured by clouds and poorly illuminated by sunlight for extended periods, remote sensing in the microwave region of the electromagnetic spectrum is the only way to observe it on an all-time basis. Second, recent work by Gloersen et al (1973, 1974) showed that it was possible by using passive microwave techniques to distinguish first-year from multiyear sea ice and to estimate ice concentrations. Third, Page and Ramseier (1975) and Campbell and Orange (1974) have shown that a variety of ice parameters, such as thickness and roughness, can be directly observed using active microwave techniques.

Because of the emphasis on microwave remote sensing all aircraft and surface effect vehicles which took part in the experiment carried one or several kinds of microwave sensors. The Argus carried an APS-94D X-band SLAR. The NASA NP-3A carried the PMIS, MFMR, and 13.3 GHz scatterometer. One surface effect vehicle carried an X-band impulse radar. Another one carried a 37.0 GHz passive microwave radiometer. A truck used to acquire ground truth data on the shore fast lake ice carried a X-band impulse radar.

We exerted great effort and considerable expense to make certain that all aircraft and most ground truth vehicles involved in this experiment carried sufficient microwave gear to allow us to accurately interpret the passive and active microwave ice data to be acquired by the S-193 radiometer-scatterometer (Rad-Scat) on board SL-4. Great efforts were also expended in making certain that all this gear was in position and operating in time for the SL-4 overpasses. Great was our disappointment then after having finished what we thought was a near perfect experiment we found that the S-193 data were useless. During this experiment the S-193 scatterometer was set to record with the transmitter off, thus no valid data were obtained. The S-193 radiometer data recorded during all of the SL-4 mission were collected with a damaged antenna the effect of which was to greatly increase the sidelobe contribution to the total integrated energy received from the sensed target and to increase the effective band width.

A study performed at the NASA Johnson Space Center (Document Number MSC-05528-SL4) compared land/water interface plots of S-193 radiometer data obtained during SL-4 with that obtained during SL-2, when the antenna was undamaged. The plot of the SL-4 brightness temperatures was observed to be smeared for more than 400 kilometers on each side of the interface giving an effective resolution element of 800 km. Thus, the only valid SL-4 brightness temperatures observed would be of homogeous targets of this scale. Since both of our study areas definately did not provide targets of this kind, we anticipated that the radiometer data would be of no use to us. Analysis of the data confirmed our anticipation.

Our disappointment over this failure to obtain S-193 data was alleviated by the excellent active and passive microwave data collected by the aircraft and ground truth vehicles. The major part of this report presents the analysis of these data. Our disappointments was also mitigated by the data collected by the other components of the EREP ensemble: the S190-A multispectral camera, the S190-B earth terrain camera, and the S192 infrared imager. Unfortunately, during four of the five EREP runs performed during the experiment the earth's surface was completely obscured by clouds. Therefore, we have one set of the above data from Orbit 83 on 14 January 1974, a day on which we were not able to make an aircraft flight. However, we did make an Argus flight one day earlier and an NP3A flight two days

following this EREP pass. Let us therefore proceed with a comparison of the EREP and aircraft data.

In Figure 17 three S190-A photographs are shown of Prince Edward Island (PEI) and it's adjacent waters. The colour infrared photograph has a spectral range of 0.5 to 0.88 microns, the colour photograph has one of 0.4 to 0.7 microns, and the black-and-white infrared photograph has one of 0.6 to 0.7 microns. At the time of observation a strong wind was blowing from the southwest and driving the pack away from the north coast of Prince Edward Island. A striking set of stratocumulus plumes can be seen forming at the ice edge and growing as they are advected northward.

Analysis of these SL-4 multispectral photographs of sea ice causes us to agree with an earlier conclusion, (Barnes and Bowley, 1974; Campbell et al, 1974a) arrived at via the analyses of sea ice imagery from Landsat-infrared and colour-infrared. These preferred bands give more information on ice types than do the lower wavelength bands. This can be seen by comparing the photographs shown in Figure 17. The ice in the zone just north of the coast, is rapidly being advected northward by the surface wind, and is composed of slush, frazil, and pancakes of light nilas. This kind of ice fills the sector north of the coast of the island. A SLAR image of this area (Dunbar and Weeks, 1975) obtained a day earlier by the Argus aircraft is given in Figure 20a. Comparison of this image with the above photograph shows the dynamic behaviour of the ice cover - the thin ice cover along the entire coast of Prince Edward Island was much further to the west only a day earlier.

The ice north and west of this band of thin ice, shown in the S190-A photographs, is made up of floes of grey-white ice and smooth grey ice. These zones which can clearly be distinguished in the infrared and colour infrared photographs, and cannot be distinguished in the colour photograph or in any of the lower wavelength photographs.

Figure 18 shows two more detailed views of the ice cover both north and south of Prince Edward Island that were obtained simultaneously with the above photographs by the S190-B Earth Terrain camera which used colour infrared film. The distinction between the slush-frazil-nilas ice zones and the grey-white and smooth grey ice zones can easily be seen in the ice cover on both sides of the island. Note how the heavier ice is being wind-driven to the east through the narrows in Northumberland Strait (south side of PEI) with the heavier ice forming a plume in the matrix of lighter ice.

An infrared image of this area of the Gulf was made by the S192 imager simultaneously with the above photographs and is shown in Figure 19. The central section of Prince Edward Island appears yellow-black (cold) and open water appears red (warm). The grey-white and smooth grey ice zones appear slightly cooler

than the slush-frazil-nilas pancake ice zones, which is what we expect since the thicker ice would be expected to have a cooler surface temperature. The lead and polynya structure shows clearly. Note how the tops of the stratocumulus plumes appear cooler than the sides. Combined infrared and visual image studies of complex ice structures reveal more ice information than studies based on single sensor images. When simultaneous microwave data are used with paired visible and infrared data, the most information can be obtained. As noted earlier, no useful microwave data were obtained by SL-4 but much excellent passive and active microwave data were obtained by aircraft over both experiment areas.

2.4 Aircraft Microwave Observations

All of the SLAR data for this experiment was obtained by the Argus aircraft using a Motorola APS-94D, X-band imager. Dunbar and Weeks (1975) present data for all of the SLAR runs shown in Figure 1 and analyze it in relation to ground truth data acquired by the CRREL team onboard the CSS Dawson (a copy of their report is included in the appendix of this report).

Figure 20 shows sections of the SLAR runs of 13 January (a) and 18 January (b) over parts of the southwest Gulf of St. Lawrence. The SLAR run of 13 January was discussed earlier in relation to the SL-4 EREP observations of orbit 83 on 14 January. What we wish to discuss in some detail here is the SLAR image of 18 January which, by a stroke of good fortune, covered an ice area which was photographed by one of the SL-4 astronauts, using the hand-held camera, during the Argus overflight. This photograph is shown as Figure 8.

This pair of images dramatically illustrates the importance of SLAR, and therefore also synthetic aperture radar (SAR), as an observation tool for floating ice research. The amount of detailed information in the SLAR image is staggering, with pressure ridges, shear ridges, floes of all sizes, plumes, etc. clearly discernable. The amount of information in the SL-4 photograph is also great, but the detail is not there. The point to be made, though, is that visible-range satellite images like this can only rarely be made, because of the predominance of cloudy weather in this region during the winter, while radar images can be obtained at any time at any desired frequency of coverage. It seems most probable that for very active, complex ice packs such as the Gulf's the only way to obtain the accurate synoptic observations at the sufficiently small time intervals needed to test numerical predictive models will be via microwave sensing.

This pair of images also illustrates a shortcoming of radar imaging of sea ice - although it is the best tool for observing structural features of all sizes it is not the best tool for observing ice types because the intensity of the return signal can not (at present) be directly related to ice age or

thickness. Some Soviet investigators (Loshchilov, personal communication) maintain that it is possible to distinguish first-year from multiyear sea ice solely using SLAR imagery while other investigators (Page and Ramseier, 1975; Dunbar, 1975; Campbell et al, 1975b) maintain that additional data is necessary. However, all investigators agree that in order to find the age of the various forms of young ice, SLAR data alone is insufficient.

For example, note on the SL-4 image two grey-white ice zones forced by the west wind against the east coast of two promontories: North Point of Prince Edward Island and Birch Point, the eastern border of Chaleur Bay. These zones appear white in the SL-4 photographs, and they were verified to be grey-white ice by trained aircraft observers. Yet in the SLAR image these zones have a weaker return signal than younger ice forms around them which have a rougher surface. The grey-white ice to the east of North Point gives a return indicating it is somewhat rough, but the strongest returns in that area are given by the interesting deformation pattern formed by the blocking effect of the island. The striking linear features that form a cone-like pattern extending two-thirds of the way across the strait appear to be shear ridges formed by the flow of ice around a blocked zone of heavier ice. They were composed of ice younger than the grey-white ice but because of their roughness gave a strong return signal. The grey-white ice trapped against the east coast of Chaleur Bay gave a much weaker return than the younger ice offshore because it was smooth.

SLAR or SAR images of sea ice when coupled with passive microwave data offer an all-weather day-or-night means for observing both ice structure and types. In order to illustrate this point we turn now to the PMIS data collected by the NASA NP-3A.

In Figure 21 through 25 we show a series of PMIS images of various sea ice types along with RC-8 photographs of selected segments of each run. The PMIS images for both the horizontal and vertical polarizations are shown with a colour code brightness temperature scale adjacent to each image. In all the PMIS illustrations the upper image is for horizontal polarization and the lower one for vertical polarization. The range of brightness temperatures for both polarizations is between 50° K to 300° K for all sea ice images and 50° K to 350° K for all lake ice images. The brightness temperature of any observation cell is found by matching its colour to the same colour on the colour scale, counting the number of colour steps to the low end (black) of the scale (composed of 70 equal steps), multiplying this number by the °K per step, and adding that number to the value of the end point. For example, for the sea ice images each step is equal to 3.59° K, thus if one counted 10 steps from the low end of the colour scale (50° K) the brightness temperature would be (3.59 x 10) + 50 = 85.9° K.

The PMIS scans at a constant angle of incidence (50 forward), therefore the images are composed of a series of parallel circular segments. The lateral scan of the system is 70 and is divided into 44 discrete steps. The system works at a frequency of 10.69 GHz and has a bandwidth of 150 MHz. The ground resolution is 150 meters from an altitude of 3050 meters. Since the altitude of the runs varied because of changes in cloud height, the resolution varies from image to image. We will therefore include a space scale at the bottom of each PMIS image. The segment of each image covered by each RC-8 photograph is also shown.

In Figure 21 we show a PMIS image and two RC-8 photographs for Run 1 on 16 January 1974, Flight 19, the location of the run being given in Figure 1. The PRT-5 infrared radiometer on board the NP-3A indicated that the surface temperature of the various ice types shown in the figure varied by not more than approximately 1 C. The initial thing that one notices on viewing these images is the great difference in brightness temperature between various ice types and between the horizontal and vertical polarizations of the same ice types.

In Figure 21b we show a photograph of a large grey-white ice floe, with an estimated thickness of 25 cm, which was the thickest ice observed from the NP-3A aircraft. The PMIS horizontal polarization gives an average brightness temperature of 240 K for the floe, while the vertical polarization gives 190 K. Note how clearly this floe shows up in the image with sharp brightness temperature gradients separating it from the ice plumes and open water mixture around it. The plume-water mixture has a representative brightness temperature of 180° K for the vertical polarization and 50 K for the horizontal polarization.

In Figure 21c we show a frazil-grey ice mixture which also is easily distinguished in the PMIS image from the plume-water mixture. The average brightness temperature of the frazil-grey ice mixture is 220 K for vertical polarization and 100 K for horizontal polarization.

Thus, the greatest variation in brightness temperature for these three ice types occur in the horizontal polarization mode, with differences of 140° K between grey-white ice and the plume-water mixture and 70° K between grey-white ice and the frazil-grey ice mixture. The ice type with the greatest variation in brightness temperature between polarizations is the plume-water mixture with a difference of 130° K.

In Figure 22 we show two PMIS images and three RC-8 photographs for the same run as in Figure 21 (these data are, however, from the northern part of the run, near Anticosti Island whereas those shown in Figure 21 are from the southern part of the run nearer to the Gaspe Peninsula). Figure 22d shows a mixture of slush and frazil with varying amounts of open water. The white area near the center of the photograph is compacted

slush and frazil with no open water (concentration 1.0), whereas the area just to the left of it shows ice of the same type but with approximately a fifth of the area open water (concentration 0.8). This difference in concentration clearly shows up in both PMIS images. In vertical polarization the high concentration has a brightness temperature of 200° K and the lower concentration has one of 140° K. In the horizontal polarization the high concentration has one of 135° K and the lower concentration has one of 90° K. Thus, for a change in concentration of approximately 20% the signature varies significantly. This is important because it indicates that in areas where the ice is uniform, it is easily possible to estimate ice concentration via microwave information.

The pancake ice shown in Figure 22c gives brightness temperatures of 210 K and 160 K in the vertical and horizontal polarizations respectively. These values are less than those for the grey-white ice and more than for the plume-water mixture observed earlier on the same run.

The grey-white ice shown in the upper part of Figure 22b has essentially the same brightness temperature in both polarization as the grey-white ice observed earlier in the same run and shown in Figure 21c.

The PMIS data discussed above was acquired on 16 January. In the five days between this NP-3A flight and the one of 21 January, the entire Gulf region was cooled vigorously by the continued advection of cold surface air from the north. The growth of ice during this period was pronounced. A PMIS image and the RC-8 photographs from Run 4 on 21 January are shown in Figure 23. The position of this run is given in Figure 1.

The rapid cooling of the surface area in this region resulted in the formation of considerable dark nilas and grey ice. An example of dark nilas is shown in the left hand side of Figure 23b; the right hand side shows older grey ice. The brightness temperature of the grey ice for vertical polarization (240° K) is about the same as for grey-white ice, but the value for horizontal polarization is considerably cooler (150 K). The transition between the nilas and the grey ice is clearly seen in the PMIS image for horizontal polarization, with brightness temperatures of 190° K and 150° K respectively, and is barely discernable in the vertical polarization image.

The bias towards a more pronounced brightness temperature difference between ice types in horizontal rather than vertical polarization is also seen between two other ice types observed in the same area and shown in Figure 23c. The upper right-hand area of the photograph shows grey-white ice which has essentially the same brightness temperature as grey-white ice observed earlier (V240° K, H190° K). An adjacent zone of heavily rafted ice, running from the lower right-hand corner towards the upper left-hand corner in Figure 22c, has brightness

temperatures of V225° K and H145° K. Thus the difference in signature between the two ice types is 45° K for the horizontal polarization and 15° K for the vertical.

In Figure 24 are shown various forms of grey ice observed on Run 3 of 21 January, the location of which is shown in Figure 1. The nilas (left) and grey ice (right) shown in Figure 21b are separated by a zone of rafted ice which is noticably cooler (30° K) in horizontal polarization than the undisturbed ice around it. The uniform grey ice shown in Figure 21c had the highest brightness temperature in vertical polarization (265° K) of all sea ice observed during this experiment. The average vertical polarization signature of the grey ice shown in Figures 21a is quite high (255° K), greater than any average for other ice types, whereas the average horizontal polarization signature (190° K) is essentially the same as for grey-white ice.

The most extensive dark nilas observed from the NP-3A aircraft was off the south side of Anticosti Island. This was the lee shore during the period of the two flights inasmuch as the wind was generally from the northwest. In Figure 25 we show a PMIS image and two RC-8 photographs from Run 1 of 21 January which covers an area on the south shore of Anticosti Island. The shorefast ice has brightness temperatures V245° K and H210° K, very similar to those of grey-white ice. What is very interesting in this case is that the shorefast ice is clearly distinguishable in the horizontally polarized PMIS image and can't be seen at all in the vertically polarized one. This is not unusual because in all other images the same ice features could be delineated in both polarizations, with the horizontal one usually giving greater differences in brightness temperature between varying ice types. This lack of feature similarity also occurs in the dark nilas just offshore from the shorefast ice zone. Once again the ice features are clearly discernable in the horizontally polarized image and poorly defined in the vertically polarized one. The average dark nilas brightness temperatures of V225° K and H125 K give a very large ΔT of 100° K. The only other ice type observed to have an equally large ΔT is frazil. Thus, it appears that the thin ice types have the greatest brightness temperature difference between polarizations.

In Table 1 we give a summary of the average brightness temperatures of the ice types observed. These data show that a wide variety of sea ice types can be distinguished using passive microwave observations. In Table 2 we show the results of an analysis of the brightness temperatures of uniform areas of ice that grew under relatively disturbed conditions, that is that all were not rafted or ridged during their drift. These results can be summarized as follows:

1) the vertically polarized brightness temperature is greater than the horizontally polarized brightness temperature for all ice types.

2) as the ice ages and becomes thicker the brightness temperature increases in both the horizontal and vertical polarizations.

3) as the ice ages and becomes thicker the difference between vertical and horizontal brightness temperatures decreases.

Table 1 - BRIGHTNESS TEMPERATURES FOR DIFFERENT ICE CONDITIONS

Fig #	V ^{o}K	H ^{o}K	V-H ^{o}K	Ice Type
21				
b	220	120	100	Frazil
b	180	50	130	Plumes - water
c	240	190	50	Grey-white
22				
b	230	200	30	Grey-white
b	225	180	45	Consolidated Pancakes
c	210	160	50	Consolidated Pancakes
d	140	90	50	Grey Slush - Open Water
d	200	155	45	White Slush
d	190	140	50	Grey Slush
23				
b	250	190	60	Nilas
b	240	150	90	Dark Nilas
c	245	200	45	Grey-White
c	225	145	80	Grey-White Rafted
24				
b	245	185	60	Thin Grey
b	255	195	60	Grey Ice
b	225	175	50	Grey Ice Rafted
c	265	195	70	Grey Ice
d	250	195	55	Grey Ice
d	245	175	70	Thin Grey
25				
b	245	210	35	Shorefast Ice
c	225	125	100	Nilas

* * *

Table 2 - AVERAGE BRIGHTNESS TEMPERATURES FOR UNIFORM ICE TYPES ACCORDING TO AGE

	V	H	ΔT
Plumes - Water	180	50	130
Frazil - Slush	220	120	100
Dark Nilas	225	125	100
Thin Grey	245	180	65
Grey	255	195	60
Grey-White	240	195	45
Shorefast	245	210	35

3. THOUSAND ISLANDS - ST. LAWRENCE RIVER

3.1 Description of Experiment

Unfortunately no Skylab-4 EREP passes were made over Lake Ontario and the Thousand Islands area of the St. Lawrence River. Some handheld camera shots of the Great Lakes area were, however, obtained by the SL-4 astronauts. A general discussion of some of these photographs can be found in Campbell et al. (1974b, 1975a). Because of the unusually light ice conditions on the lakes at the time of the overpasses they proved to be not too useful in the limited area of the experiment in contrast to the photographs that were obtained of the Gulf of St. Lawrence. The NASA NP-3A aircraft did make one flight over the area on February 4, the tracks of which are shown in Figure 26. The flight lines 1 and 2 did extend about 40 miles further down river to the Prescott-Ogdensburg area. This is not shown in the Figure. The key sensors used in this flight were the PMIS and the two RC-8 cameras.

Detailed ground truth observations were obtained along parts of lines 4, 5 and line 6, and general ground truth observations were made along the entire length of lines 1 and 2.

3.2 Ice Regime

The initial freezing occured on January 8, but the thin clear ice layer that formed broke up quickly as a result of high winds. A continuation of these high winds, combined with low temperatures, then created large amounts of slush in the river. When the wind dropped on 12 January, this froze immediately forming a continuous ice cover over most of the river except at places with high water velocities. Continued cold air temperatures then caused a steady growth of the secondary ice cover. Figure 27 shows the meteorological data for the Kingston area as obtained from the Atmospheric Environment Service.

Frequent, but not heavy snowfalls caused a small buildup of superimposed ice, which peaked in thickness by January 20. Following this, mild weather with frequent rain was experienced. The ice surface had melted significantly when a record high temperature combined with high southwesterly winds on January 27 rapidly destroyed this river ice cover by January 30. The lake ice cover which extended to Main Duck Island broke up, and accumulated as rafted ice in the river entrance as well as down river.

By early February, calm weather and low temperatures caused the river to refreeze, with the secondary ice cover on 75% of the river averaging 15cm thickness by February 5. A steady growth of this secondary layer continued until mid-February, with some light snow again building a small superimposed cover, which reached a maximum around February 20. During the latter part of

February a warming trend was experienced and these above freezing temperatures rapidly deteriorated the superimposed ice layer and caused steady melting of the secondary ice cover. By March 5 rain and above freezing temperatures combined with high winds, had destroyed most of the ice cover. Only areas of heavy, rafted ice remained in the Alexandria Point-Cape Vincent section. Continued mild weather caused this ice to break further and no ice was left in this section of the river by March 13, 1974. A more detailed description of the ice regime in the St. Lawrence River is given by Ramseier and Weaver (1974). Throughout the winter season the thickness was monitored by using 19 ice thickness gauges (Ramseier and Weaver, 1975) extending along sight lines 1 and 2. Figure 28 shows four ice thickness profiles. The location of each profile is indicated on Figure 26, except for station H-3 which is located just above the Prescott-Ogdensburg area at km 9.65. The profiles have been plotted to show how much of the total ice thickness is due to secondary growth (uniform ice growth into the river parallel to the direction of heat flow) and to superimposed ice (formed from snow and water on top of the existing ice cover). A detailed description of the different river and lake ice types is given by Michel and Ramseier (1970).

As can be seen from the profiles the ice thickness varies greatly over the season. It is also quite evident that only a small amount of superimposed ice was present during the NP-3A overflight on February 4. At first glance this might not seem too important. However the large air bubbles which commonly occur in superimposed ice act as scatterers causing the brightness temperature to vary significantly.

The ice conditions on February 4 were quite ideal because the ice cover was snow free. This facilitated the comparisons between the PMIS data and the RC-8 photography.

3.3 Ground Truth and Aircraft Observations

Detailed ground truth measurements were obtained along the southwest end of line 4, the west end of line 5, along line 6, and at intermediate locations along lines 7 and 2 (see Figure 26 for the locations of these lines). The measurements consisted of ice thickness, ice type, ice structure and texture. The ice thicknesses were also measured with an X-band impulse radar (Chudobiak et al., 1974). In addition, the surface brightness temperatures were obtained by Aerojet Electrosystems along lines 4 and 6 using a 37 GHz passive microwave radiometer. The measurements were made of the surface with the radiometer and the X-band radar mounted on air cushion vehicles. The setup for the X-band impulse radar is shown in Figure 29A and for the passive microwave system in Figure 29A.

Flight line 1 (Figure 26) was flown at an altitude of 2225 metres. Two partial mosaics have been prepared showing the two types of contrasting but general ice conditions. Figure 30 shows a stretch of river extending 13 km from Ogdensburg (bottom

right hand corner of RC-8 mosaic) up river to Morristown (bottom left hand side of RC-8 mosaic). The ice conditions along the centre of the St. Lawrence River, which represents part of the international section of the seaway, are rather uniform. The ice cover was generally composed of black ice with an average thickness of 0.15 m. The black spots in the RC-8 imagery represent open water and the whitish areas on the west side of the open water features represents frost on top of black ice. In some cases part of the open water areas also contain frazil slush. The scalloped edge of the ice cover between Ogdensburg and Prescott is due to the presence of an ice boom which retains the ice up river. The white band along the entire U.S. shore represents shorefast ice or ice which formed during the first period of the winter.

The 10.69 GHz PMIS imagery, corresponding to the RC-8 colour mosaic, shows rather clearly the uniform ice conditions. The bottom strip shows the difference between the V and H polarized brightness temperatures.

The brightness temperatures V 180° K and H 120° K of the black fresh water ice are substantially different from the V 225 K and H 125 K of the dark nilas sea ice. This is to be expected since the microwave emission of these two kinds of ice varies greatly due to the differing dielectric properties of each medium. The dielectric properties of black fresh water ice are well understood (Vant et al., 1974) but for all other forms of fresh water ice they are poorly understood. The dielectric properties of sea ice, which is a much more complex dielectric medium than fresh water ice because of the effects of the salt trapped within it, are reasonably understood for first-year and younger ice forms but poorly understood for multiyear ice. The interpretation of passive microwave signatures of sea ice is far more advanced than fresh ice because of the large amount of work that has been carried out in recent years, notably by the AIDJEX (Arctic Ice Dynamics Joint Experiment) - NASA remote sensing program and the BESEX (Bering Sea Experiment) Program.

Both the horizontally and vertically polarized images in Figure 30 show shorelines that are easily distinguishable from both ice and open water. The superimposed ice trapped by the ice boom at Prescott-Ogdensburg has brightness temperatures of V 220° K and H 150° K and also clearly discernable in both images. Figure 31 shows a plot of the average brightness temperatures along the centerline of the St. Lawrence River from Prescott-Ogdensburg to Lake Ontario as well as a plot of ice thickness along the same line. As one preceeds upstream from the superimposed ice at Prescott-Ogdensburg, the black ice thickness gradually increases reaching a thickness of 18 cm at 10 km. In this same zone as the ice thicknesses increase upstream, both the horizontal and vertical polarization brightness temperatures increase and then remain generally constant over the uniform thickness black ice cover that is further upstream. An example of such a uniform area of black ice is shown in Figure 37A. This ice

shown is about 0.15 m thick and is comprised of secondary ice having a columnar crystal structure.

Proceeding upstream we note that both brightness temperatures start increasing at approximately 20 km downstream from Cape Vincent and gradually reach peak values of V 230° K and H 180° K at the ice arch at Tibbett Point. This area is shown in the photograph in Figure 32. The area of brightness temperatures that are warmer then those for black ice is composed of fractured and refrozen ice (shown in Figure 37B). The underwater ice ridge just beyond Cape Vincent (shown in Figure 31 at 10.8 cm) is also seen in Figure 37C. This area of deformed ice corresponds to high brightness temperatures of V 230° K and H 180° K.

Figure 32 shows PMIS images and photographs of the ice cover of the eastern end of Lake Ontario at the entrance to the St. Lawrence River. These data were acquired on the same run as those shown in Figures 30 and 31. At the time of observation a cold wind was blowing from the NE, almost upriver. In this situation the area west of the Tibbetts Point ice arch becomes an ice generating region. This is clearly seen in the photomosaic shown in Figure 32. Bands of slush-frazil were formed just east of the ice arch and advected westwards by the strong surface wind. As they moved they increased in thickness. The slush-frazil bands close to the ice arch were 1-2 cm thick while those near the black ice were 5 cm thick. The slush-frazil bands show up far more distinctly in the horizontally polarized image than in the vertical one. The transition from these bands into the black ice is clearly discernable in both images. It is interesting to note that the horizontally polarized image and the 4T image (Figure 32) could serve as almost duplicate ice feature maps.

In Figure 33 we show PMIS images and a photomosaic for line 4 of 4 February in the vicinity of Carleton Island. Three distinct ice forms are clearly delineated in the PMIS image. Just north of Carleton Island, adjacent to the coast, is a zone made up of a mixture of refrozen floes of fractured black ice that has a brightness temperature of V 225° K and H 175° K. Just north of this zone and adjacent to it is a zone composed of frozen slush-frazil, having a brightness temperature of V 240° K and H 200° K. To the east of Carleton Island is a large area of relatively undisturbed black ice that has brightness temperatures of V 170° K and H 105° K. These three zones are delineated about equally well in the horizontally and vertically polarized images.

Line 4 ended in Button Bay, and Figure 34 shows both PMIS images and a photomosaic of that area. Four distinct ice zones can be delineated. The ice in Button Bay rested on the bottom and has a distinctly different horizontally polarized microwave signature (V 215° K, H 160° K) than the floating shorefast ice (V 215° K, H 130° K) adjacent to it. The first black ice zone, adjacent to the shorefast ice, shows up equally well in both polarizations (V 170° K, H 100° K) as does the second black ice zone (V 190° K, H 110° K) on the other side of

the refrozen lead. It is interesting that all the floating ice forms shown have approximately the same thickness. Figure 35 shows a thickness profile that runs along the centerline of the images and photomosaic shown in Figure 34. Station 1 is at the entrance to Button Bay, station 11 is at the offshore edge of the shorefast ice, and station 33 is at the end of the black ice. Unlike sea ice, lake ice can remain as black ice up to extreme thickness as long as it grows undisturbed.

We also show in Figure 35 centerline profiles of the PMIS data and the 37 GHz data acquired from a surface effect vehicle. The transition from shorefast ice to black ice appears in both polarizations for both frequencies but is much more pronounced for the lower frequency (10.69 GHz) of the PMIS.

A final profile along line 6 is shown in Figure 36. The flight line extended from Wolfe Island to Kingston. The ice there was somewhat more irregular, with the thickest portions occurring near Wolfe Island and containing about 50% snow ice. The brightness temperatures from the PMIS measurements are initially very high near the coast of Wolfe Island. However they drop off rapidly as one moves farther north of the Island. Part of this drop off is undoubtedly caused by the decrease in ice thickness as one moves between station 1 to station 3. After station 15 there is again a slight increase in the 10.69 GHz brightness temperature as one moves further north toward Kingston. This is believed to coincide with the increased presence of black ice.

We believe that this preliminary assessment of the PMIS data indicates that its potential application to lake ice is as great as its application to sea ice in that many different forms of lake ice can be distinguished. Also as for sea ice, the horizontal polarization gives greater signature contrast between ice types and a sharper delineation of ice features.

4. CONCLUSIONS

In this paper we have described in considerable detail the Skylab-4 Floating Ice Experiment. This was a complex experiment, particularly from an operational view point, in that it required coordination between the satellite, two aircraft, and ground truth parties operating from a ship in the Gulf of St. Lawrence and from three hovercraft on the St. Lawrence River. The satellite contribution to the program was greatly decreased because of the failure of the S-193 radiometer-scatterometer to collect valid data. This was most unfortunate inasmuch as most of the ground truth program was designed to contribute information needed for the interpretation of these results. However we did find the hand-held photography taken from the satellite to be most useful in providing an overall view of the rapid changes in ice conditions in the Gulf.

The coupling of the aircraft data with the ground truth observations proved to be highly successful with interesting

results being obtained with IR and SLAR (see also Dunbar and Weeks, 1975) passive microwave techniques, and standard photography. Of particular interest were the results of the PMIS system which operated at 10.69 GHz with both vertical and horizontal polarizations. This was the first time that dual polarized images have been obtained from floating ice. In both sea and lake ice it was possible to distinguish a wide variety of thin ice types because of their large differences in brightness temperatures. It was found that (a) the higher brightness temperature was invariably obtained in the vertically polarized mode, and (b) as the age of the ice increases the brightness temperature increases in both polarizations. Associated with this change in age (c) the difference in temperature as observed by the different polarizations decreased. In general it appears that (d) the horizontally polarized data is the most sensitive to variations in ice type for both fresh water ice and sea ice. The study also showed the great amount of information on ice surface roughness and deformation patterns that can be obtained from X-band SLAR observations. Our experience on this experiment has served to reinforce the opinion we expressed in Campbell et al. (1975) that the best all-weather floating ice remote sensing data can be obtained via the combined operation of passive and active microwave systems.

6. ACKNOWLEDGEMENTS

This study required the use and coordination of a complex array of scientific vehicles--the Skylab-4 laboratory, the Canadian Argus aircraft, the U.S. NP-3A aircraft, the Canadian oceanographic vessel CSS Dawson, a Canadian helicopter, and three Canadian hovercraft--operating on and over two extensive waterways during the season of their most inclement weather. We wish to thank all of the many scientists, technicians, and administrators who have helped us and we wish to specifically thank the following:

- Colonel Gerald Carr, Dr. Edward Gibson, and Colonel William Pogue, the Skylab-4 astronauts, for their whole-hearted support of this experiment before, during, and following their historic space flight;
- the crew of the Canadian Argus remote sensing aircraft;
- the crew of the U.S. NP-3A remote sensing aircraft;
- Dr. W.D. Forrester and the crew of the CSS Dawson;
- Robert Gray, Floyd Kugzruk, David Meeks, Joseph Montgomery, Archie Staley, Stephen Taylor, Mrs. Cory Van Hal, and Murray Wongkee for their fine work on a difficult ground truth program;

- Dr. Olav Loken, Dept. of the Environment, for helping us obtain the extensive Canadian support for this experiment.

- and the Arctic Program, U.S. Office of Naval Research for funding the ground truth program for the Gulf of St. Lawrence.

7. REFERENCES

Barnes, J.C. and C.J. Bowley (1974) The application of ERTS imagery to monitoring Arctic sea ice. Environmental Research and Technology, Inc., Lexington, Mass., ERT Document 0408-F.

Campbell, K.J. and A.S. Orange (1974) A continuous profile of sea ice and freshwater ice thickness by impulse radar. Polar Record 17(106), 31-41.

Campbell, W.J., P. Gloersen, W. Nordberg and T.T. Wilheit (1974a) Dynamics and morphology of Beaufort Sea ice determined from satellites, aircraft, and drifting stations, in COSPAR Approaches to Earth survey problems through use of space techniques (P. Brock and others, eds.), Akademie-Verlag, Berlin. 311-27 (Konstanz, F.R.G.)

Campbell, W.J., R.O. Ramseier, W.F. Weeks and J.A. Wayenberg (1974b) Preliminary results of lake and sea ice experiment, in Skylab-4 Visual Observations Project (J.L. Kaltenback et al., eds.), NASA Technical Memorandum TMX-58142, JSC-09053, L.B. Johnson Space Center, Houston, Texas, p. 11.1-11.10.

Campbell, W.J., R.O. Ramseier, W.F. Weeks and J.A. Wayenburg (1975a) Visual observations of floating ice from Skylab. Skylab Visual Observation Project Rept. No. 2, L.B. Johnson Space Center, Houston, Texas.

Campbell, W.J., W.F. Weeks, R.O. Ramseier and P. Gloersen (1975b) Geophysical studies of floating ice by remote sensing. J. Glaciol. 15(73), 305-328.

Campbell, W.J., R.O. Ramseier, W.F. Weeks, and P. Gloersen (1976) An integrated approach to the remote sensing of sea ice. Proceed. Third Canad. Sympos. on Remote Sensing (Edmonton, Alta., October 1975).

Chudobiak, W.J., R.B. Gray, R.O. Ramseier, V. Makios, M. Vant, J.L. Davies and J. Katsube (1974) Radar remote sensors for ice thickness and soil moisture measurements. Proceed. Second Canad. Sympos. on Remote Sensing. (Guelph, Ontario, 418-424.

Dunbar, M. (1975) Interpretation of SLAR imagery of sea ice in Nares Strait and the Arctic Ocean. J. Glaciol. 15(73), 373-89.

Dunbar, M. and W.F. Weeks (1975) Interpretation of young ice forms in the Gulf of St. Lawrence using side-looking airborne radar and infrared imagery. Cold Regions Research and Engineering Laboratory Research Rept. 337, 41pp.

Gloersen, P., W. Nordberg, T.J. Schmugge, T.T. Wilheit and W.J. Campbell (1973) Microwave signatures of first-year and multiyear sea ice. J. Geophys. Res. 78(18), 3564-72.

Gloersen, P., T.C. Chang, T.T. Wilheit and W.J. Campbell (1974) Polar sea ice observations by means of microwave radiometry; in ''Advanced Concepts and Techniques in the Study of Snow and Ice Resources'' (H.S. Santeford and J.L. Smith, comps). Natl. Acad. Sciences, Washington, D.C. p. 541-550.

Michel, B. and R.O. Ramseier (1970) Classification of river and lake ice. Canad. Geotechnical Journal 8, 36-45.

Page, D.F. and R.O. Ramseier (1975) Applications of active radar techniques to the study of ice and snow. J. Glaciol. 15(73), 171-91.

Ramseier, R.O. and R.J. Weaver (1974) Ice information, Montreal-Lake Ontario Section, St. Lawrence River. In: Navigation Season Extension studies, Gulf of St. Lawrence to Great Lakes Winter 1973-74. Canadian Marine Transportation Administration, Transport Canada, p. 1-17.

Ramseier, R.O. and R.J. Weaver, (1975) Floating ice thickness and structure determination heated wire technique. Technical Bulletin No. 88, Environment Canada, Inland Waters Directorate, Ottawa 16pp.

Vant, M.R., R.B. Gray, R.O. Ramseier and V. Makios (1974) Dielectric properties of fres h and sea ice at 10 and 35 GHz. J. Appl. Phys. 45(11), 4712-7; erratum J. Appl. Phys. 46(5), 2339.

8. FIGURE CAPTIONS

1. Map or Gulf of St. Lawrence showing SL-4, aircraft and ship paths.

2. Ice photographs from CSS Dawson

   a) Pancake ice near soth coast of St. Lawrence River estuary

   b) Grey ice near south shore of St. Lawrence River estuary

   c) Pressure ridging in the Gulf of St. Lawrence

   d) Ice plumes near the edge of the St. Lawrence ice pack (aerial view)

   e) Ice plumes near the edge of the St. Lawrence ice pack (surface view)

3. SL-4 photograph - NW part of Gulf of St. Lawrence
   6 January 1974 - 139-3934

4. SL-4 photograph - NE part of Gulf of St. Lawrence
   Straits of Belle Isle
   11 January 1974 - 139-4072

5. SL-4 photograph - NE part of Gulf of St. Lawrence
   Straits of Belle Isle
   19 January 1974 - 141-4268

6. SL-4 photograph - NE part of Gulf of St. Lawrence
   E part Straits of Belle Isle
   20 January 1974 - 141-4326

7. SL-4 photograph - Gulf of St. Lawrence
   20 January 1974 - 141-4331

8. SL-4 photograph - W Gulf of St. Lawrence Gaspe Peninsula
   18 January 1974 - 140-4215

9. SL-4 photograph - W Gulf of St. Lawrence Gaspe Peninsula
   20 January 1974 - 141-4321

10. SL-4 photograph - NW Gulf of St. Lawrence
    Anticosti Island
    18 January 1974 - 140-4216

11. SL-4 photograph - NW Gulf of St. Lawrence
    Anticosti Island
    20 January 1974 - 141-4327

12. SL-4 photograph - N Central Gulf of St. Lawrence
    Anticosti Island
    21 January 1974 - 141-4366

13. Ice Reconnaissance Map of Gulf of St. Lawrence, 8 January

14. Ice Reconnaissance Map of Gulf of St. Lawrence, 13 January

15. Ice Reconnaissance Map of Gulf of St. Lawrence, 18 January

16. Ice Reconnaissance Map of Gulf of St. Lawrence, 22 January

17. Three S190-A Multispectral Camera photographs of the Prince Edward Island area of the Gulf of St. Lawrence taken on 14 January 1974. The spectral ranges of each photograph are as follows:

    Colour - 0.4 to 0.7 microns
    Colour IR - 0.5 to 0.88 microns
    IR - 0.6 to 0.7 microns

18. Two S190-B Earth Terrain Camera photographs of the Prince Edward Island area of the Gulf of St. Lawrence taken on 14 January 1974.

19. S192 infrared image of the Prince Edward Island area of the Gulf of St. Lawrence taken on 14 January 1974.

20. Two X-band side-looking airborne radar (SLAR) images of portions of the Gulf of St. Lawrence obtained by the Argus aircraft. (a) was taken on 13 January 1974 with a swath width of 50 km. (b) was taken on 18 January 1974 with a 25 km. swath width. The location of these SLAR runs is shown in Figure 1.

21. PMIS image and RC-8 photographs for Run I, Flight 19 on 16 January 1974 of the NASA NP-3A aircraft. The location of this run is shown in Figure 1.

    a) PMIS image

    b) Ice plumes and frazil - grey ice mixture

    c) Grey-white ice

22. PMIS image and RC-8 photographs for Run I, Flight 19 on 16 January 1974 of the NASA NP-3A aircraft. The location of this run is shown in Figure 1.

    a) PMIS image

    b) Consolidated pancake and grey-white ice

    c) Pancake ice

    d) Slush and frazil

23. PMIS image and RC-8 photographs for Run 4, Flight 24 on 21 January 1974 of the NASA NP-3A aircraft. The location of this run is shown in Figure 1.

    a) PMIS image

    b) Nilas and grey ice

    c) Grey-white and rafted ice

24. PMIS image and RC-8 photography for Run 3, Flight 24 on 21 January 1974 of the NASA NP-3A aircraft. The location of this run is shown in Figure 1.

    a) PMIS image

    b) Nilas and grey ice

    c) Grey ice

    d) Grey ice and nilas

25. PMIS image and RC-8 photography for Run 1, Flight 24 on 21 January 1974 on the NASA NP-3A aircraft. The location of this run is shown in Figure 1.

    a) PMIS image

    b) Shorefast ice

    c) Nilas

26. Map of St. Lawrence River-Thousand Islands area showing aircraft flight lines.

27. Meteorological data of the Thousand Islands area showing windspeed and direction, daily maximum and minimum air temperatures and the amount of snow precipitation.

28. Ice thickness station profiles showing the thickness due to secondary and superimposed ice. A) Station H-3 9.65 km; B) Station 6 78.8 km; C) Station 12 99.7 km and D) Station 17 102.2 km from Prescott-Ogdensburg.

29. Part A shows the air-cushion vehicle on which the horn of the X-band impulse radar is visible. The generator for the power supply is mounted on the opposite side of the antenna on top of the frame. The ACV is sitting on top of black ice (secondary ice) surrounded by patches of white superimposed ice (snow ice) on top of secondary ice.

Part B shows the ACV with Aerojet Electrosystems 37 GHz passive microwave radiometer. In this particular setup the brightness temperature was determined as a function of ice thickness (during the growth of secondary ice).

30. Photomosaic and PMIS imagery of part of the St. Lawrence River - Morristown to Ogdensburg. This data was obtained along flight line 1 at an altitude of 2225 m on February 4, 1974.

31. Ice thickness and PMIS brightness temperature profile along flight line 1.

32. Photomosaic and PMIS imagery of Tibbetts Point and Lake Ontario along the beginning of line 1, taken at an altitude of 700 m.

33. Photomosaic and PMIS imagery along line 4 north of Carleton Island, taken at an altitude of 700 m.

34. Photomosaic and PMIS imagery at the end of line 4 over Button Bay taken at an altitude of 700 m.

35. Ice thickness and brightness temperature profiles for 10.69 GHz and 37 GHz. PMIS and Aerojet passive microwave radiometers respectively. This area corresponds to the shorefast and black ice area in Figure 34.

36. Ice thickness and brightness temperature profiles for 10.69 GHz and 37 GHz PMIS and Aerojet passive microwave radiometer respectively. These profiles correspond to flight line 6.

37. Surface photographs of some distinct ice conditions

    a) Black ice

    b) Refrozen ice floe field

    c) Ridge at Lake Ontario - St. Lawrence River interface.

9. APPENDIX

Anchor ice: Submerged ice attached or anchored to the bottom, irrespective of the nature of its formation.

Bergy bit: A large piece of floating glacier ice, generally showing less than 5 m above sea-level but more than 1 m and normally about 100-300 sq. m in area.

Brash ice: Accumulations of floating ice made up of fragments not more than 2 m across, the wreckage of other forms of ice.

Bummock: From the point of view of the submariner, a downward projection from the underside of the ice canopy; the counterpart of a hummock.

Close Pack ice: Pack ice in which the concentration is 10/10 to 8/10 (6/8 to less than 7/8), composed of floes mostly in contact.

Compact pack ice: Pack ice in which the concentration is 10/10 (8/8) and no water is visible.

Concentration: The ratio in tenths of the sea surface actually covered by ice to the total area of sea surface, both ice-covered and ice-free, at a specific location or over a defined area.

Consolidated pack ice: Pack ice in which the concentration is 10/10 (8/8) and the floes are frozen together.

Dark nilas: Nilas which is under 5 cm in thickness and is very dark in colour.

Diverging: Ice fields or floes in an area are subjected to diverging or dispersive motion, thus reducing ice concentration and/or relieving stresses in the ice.

Fast ice: Sea ice which forms and remains fast along the coast, where it is attached to the shore, to an ice wall, to an ice front, between shoals or grounded icebergs. Vertical fluctuations may be observed during changes of sea-level. Fast ice may be formed in situ from sea water or by freezing of pack ice of any age to the shore, and it may extend a few metres or several hundred kilometres from the coast. Fast ice may be more than one year old and may then be prefixed with the appropriate age category old, second-year, or multi-year. If it is thicker than above 2 m above sea-level it is called an ice shelf.

Fast-ice boundary: The ice boundary at any given time between fast ice and pack ice.

First-year ice: Sea ice of not more than one winter's growth, developing from young ice; thickness 30 cm - 2 m. May be subdivided into thin first-year white ice, medium first-year ice and thick first-year ice.

Flaw: A narrow separation zone betwen pack ice and fast ice, where the pieces of ice are in chaotic state; it forms when pack ice shears under the effect of a strong wind or current along the fast ice boundary.

Floating ice: Any form of ice found floating in water. The principal kinds of floating ice are lake ice, river ice, and sea ice, which forms by the freezing of water at the surface, and glacier ice (ice of land origin) formed on land or in an ice shelf. The concept includes ice that is stranded or grounded.

Floe: Any relatively flat piece of sea ice 20 m or more across. Floes are subdivided according to horizontal extent as follows:

GIANT: Over 10 km across
VAST: 2-10 km across
BIG: 500-2,000 m across
MEDIUM: 100-500 m across
SMALL: 20-100 m across

Floeberg: A massive piece of sea ice composed of a hummock, or a group of hummocks, frozen together and separated from any ice surroundings. It may float up to 5 m above sea-level.

Fracture: Any break or rupture through very close pack ice, compact pack ice, consolidated pack-ice, fast ice, and/or be covered with nilas and/or young ice. Length may vary from a few metres to many kilometres.

Frazil ice: Fine spicules or plates of ice, suspended in water.

Glacier: A mass of snow and ice continuously moving from higher to lower ground or, if afloat, continuously spreading. The principal forms of glacier are: inland ice sheets, ice shelves, ice streams, ice caps, ice pied-monts, cirque glaciers and various types of mountain (valley) glaciers.

Glacier ice: Ice in, or originating from a glacier, whether on land or floating on the sea as icebergs, bergy bits or growlers.

Grease ice: A later stage of freezing than frazil ice when the crystals have coagulated to form a soupy layer on the surface. Grease ice reflects little light, giving the sea a matt appearance.

Grey ice: Young ice 10-15 cm thick. Less elastic than nilas and breaks on swell. Usually rafts under pressure.

Grey-white ice: Young ice 15-30 cm thick. Under pressure more likely to ridge than to raft.

Growler: Smaller piece of ice than a bergy bit or floeberg, often transparent but appearing green or almost black in colour, extending less than 1 m above the sea surface and normally occupying an area of about 20 sq. m.

Hummock: A hillock of broken ice which has been forced upwards by pressure. May be fresh or weathered. The submerged volume of broken ice under the hummock, forced downwards by pressure, is termed a bummock.

Iceberg: A massive piece of ice of greatly varying shape, more than 5 m above sea-level, which has broken away from a glacier, and which may be afloat or aground. Icebergs may be described as tabular, dome-shaped, sloping, pinnacled, weathered or glacier bergs.

Ice boundary: The demarcation at any given time betwen fast ice and pack ice or between areas of pack ice of different concentrations.

Ice canopy: Pack ice from the point of view of the submariner.

Ice cover: The ratio of an area of ice of any concentration to the total area of sea surface within some large geographic local; this local may be global, hemispheric, or prescribed by a specific oceanographic entity such as Baffin Bay or the Barents Sea.

Ice field: Area of pack ice consisting of any size of floes, which is greater than 10 km across.

Ice-free: No sea ice present. There may be some ice of land origin.

Ice front: The vertical cliff forming the seaward face of an ice shelf or other floating glacier varying in height from 2-50 m or more above sea level.

Ice keel: From the point of view of the submariner, a downward projecting ridge on the underside of the ice canopy; the counterpart of a ridge. Ice keels may extend as much as 50 m below sea-level.

Ice of land origin: Ice formed on land or in an ice shelf, found floating in water. The concept includes ice that is stranded or grounded.

Ice rind: A brittle shiny crust of ice formed on a quiet surface by direct freezing or from grease ice, usually in water of low salinity. Thickness to about 5 cm. Easily broken by wind or swell, commonly breaking in rectangular pieces.

Ice shelf: A floating ice sheet of considerable thickness showing 2-50 m or more above sea level, attached to the coast. Usually of great horizontal extent and with a level or gently undulating surface. Nourished by annual snow accumulation and often also by the seaward extension of land glaciers. Limited areas may be aground. The seaward edge is termed an ice front.

Ice stream: Part of an inland ice sheet in which the ice flows more rapidly and not necessarily in the same direction as the surrounding ice. The margins are sometimes clearly marked by a change in direction of the surface slope but may be indistinct.

Ice wall: An ice cliff forming the seaward margin of a glacier which is not afloat. An ice wall is aground, the rock basement being at or below sea-level.

Lake ice: Ice formed on a lake, regardless of observed location.

Lead: Any fracture or passage-way through sea ice which is navigable by surface vessels.

Light nilas: Nilas which is more than 5 cm in thickness and rather lighter in colour than dark nilas.

Medium first-year ice: First-year ice 70-120 cm thick.

Multi-year ice: Old ice up to 3 m or more thick which has survived at least two summers' melt. Hummocks even smoother than in second-year ice, and the ice is almost salt-free. Colour, where bare, is usually blue. Melt pattern consists of large interconnecting irregular puddles and a well-developed drainage system.

Nilas: A thin elastic crust of ice, easily bending on waves and swell and under pressure, thrusting in a pattern of interlocking "fingers" (finger rafting). Has a matt surface and is up to 10 cm in thickness. May be subdivided into dark nilas and light nilas.

Old Ice: Sea ice which has survived at least one summer's melt. Most topographic features are smoother than on first-year ice. May be subdivided into second-year ice and multi-year ice.

Pack ice: Term used in a wide sense to include any area of sea ice, other than fast ice, no matter what form it takes or how it is disposed.

Pancake ice: Predominantly circular pieces of ice from 30 cm - 3 m in diameter, and up to about 10 cm in thickness, with raised rims due to the pieces striking against one another. It may be formed on a slight swell from grease ice, shuga or slush or as a result of the breaking of ice rind, nilas or, under severe conditions of swell or waves, of grey ice. It also sometimes forms at some depth, at an interface between water bodies of different physical characteristics, from where it floats to the surface; its appearance may rapidly cover wide areas of water.

Rafted ice: Type of deformed ice formed by one piece of ice overriding another.

Ridge: A line or wall of broken ice forced up by pressure. May be fresh or weathered. The submerged volume of broken ice under a ridge, forced downwards by pressure, is termed an ice keel.

River ice: Ice formed on a river, regardless of observed location.

Sea ice: Any form of ice found at sea which has originated from the freezing of sea water.

Second-year ice: Old ice which has survived only one summer's melt. Because it is thicker and less dense than first-year ice, it stands higher out of the water. In contrast to multi-year ice, summer melting produces a regular pattern of numerous small puddles. Bare patches and puddles are usually greenish-blue.

Shearing: An area of pack ice is subject to shear when the ice motion varies significantly in the direction normal to the motion, subjecting the ice to rotational forces. These forces may result in phenomena similar to a flaw.

Shuga: An accumulation of spongy white ice lumps, a few centimetres across; they are formed from grease ice or slush and sometimes from anchor ice rising to the surface.

Slush: Snow which is saturated and mixed with water on land or ice surfaces, or as a viscous floating mass in water after a heavy snowfall.

Thick first-year ice: First-year ice over 120 cm thick.

Thin first-year ice/white ice: First-year ice 30-70 cm thick.

White ice: See Thin first-year ice.

Young ice: Ice in the transition stage betwen nilas and first-year ice, 10-30 cm in thickness. May be sub-divided into grey ice and grey-white ice.

*Black ice: Transparent ice formed in rivers and lakes (similar to dark nilas).

*Ice plume: Elongated area of slush or small ice flows that is stretched out parallel to the wind direction existing in open water areas.

*Vortex: A whirl of ice floes or brash in open water areas.

*Definitions not contained in WMO Sea-Ice Nomenclature.

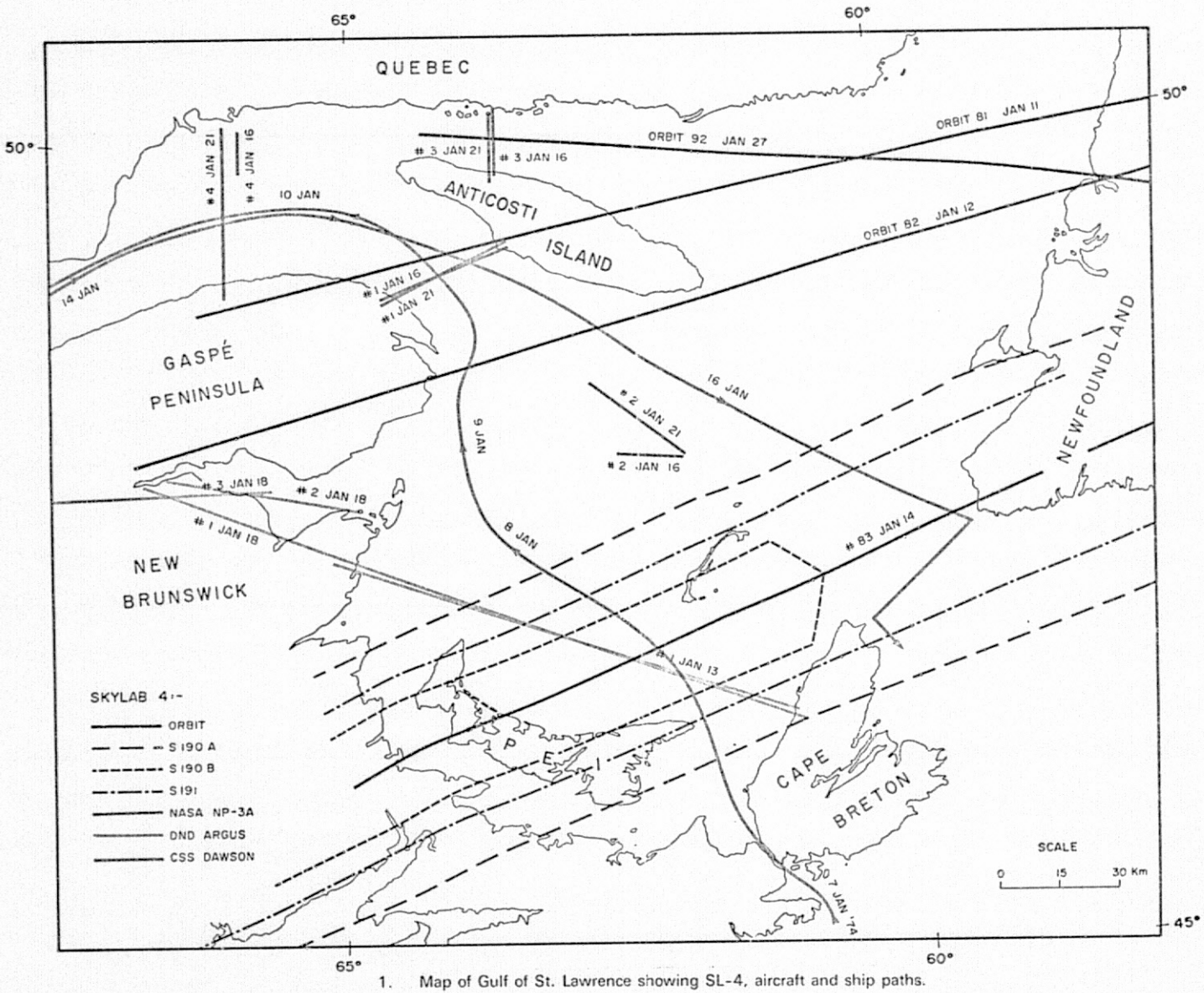

1. Map of Gulf of St. Lawrence showing SL-4, aircraft and ship paths.

2. Ice photographs from CSS Dawson

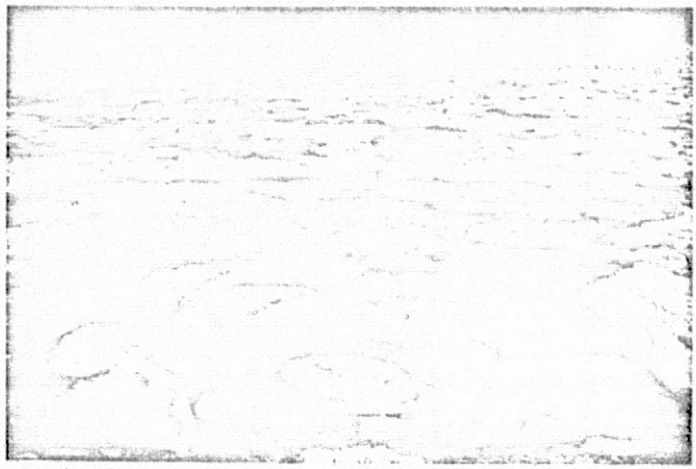

a) Pancake ice near south coast of St. Lawrence River estuary

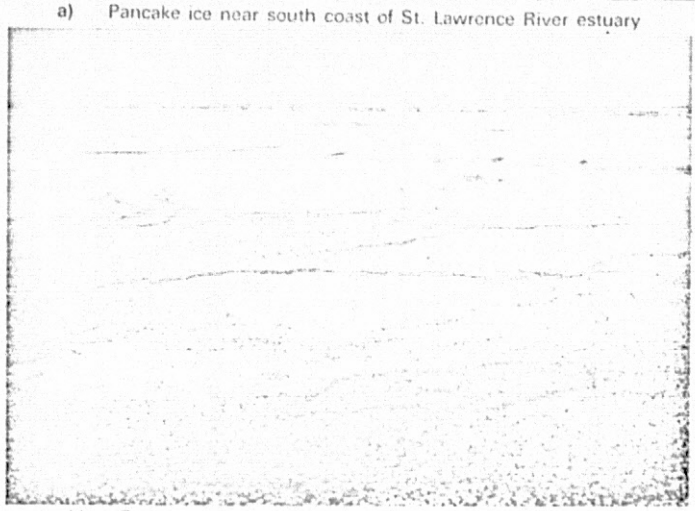

b) Grey ice near south shore of St. Lawrence River estuary

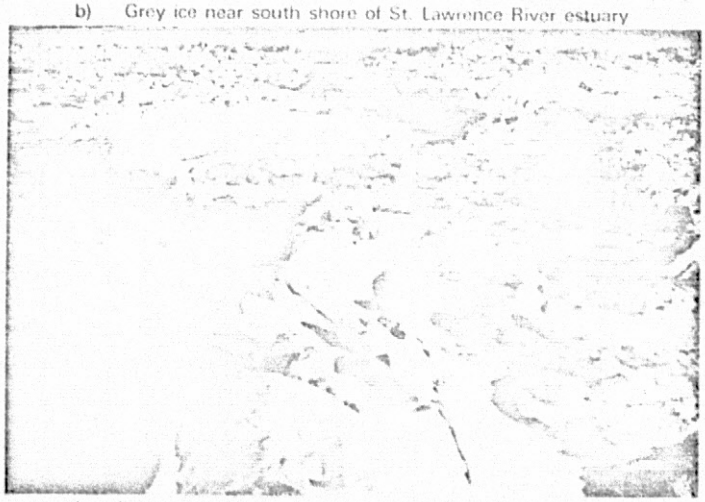

c) Pressure ridging in the Gulf of St. Lawrence

d) Ice plumes near the edge of the St. Lawrence ice pack (aerial view)

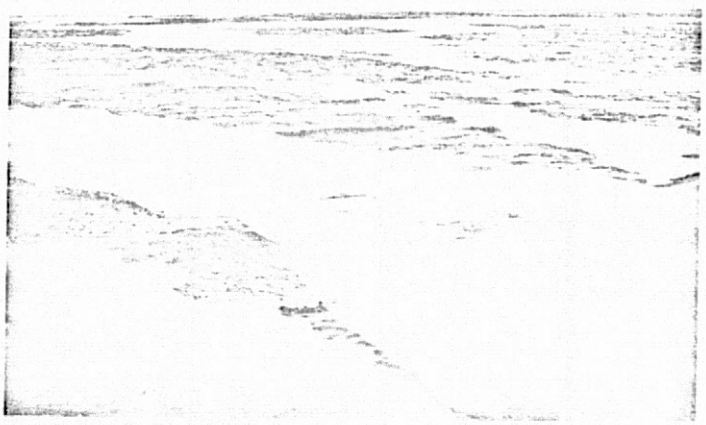

e) Ice plumes near the edge of the St. Lawrence ice pack (surface view)

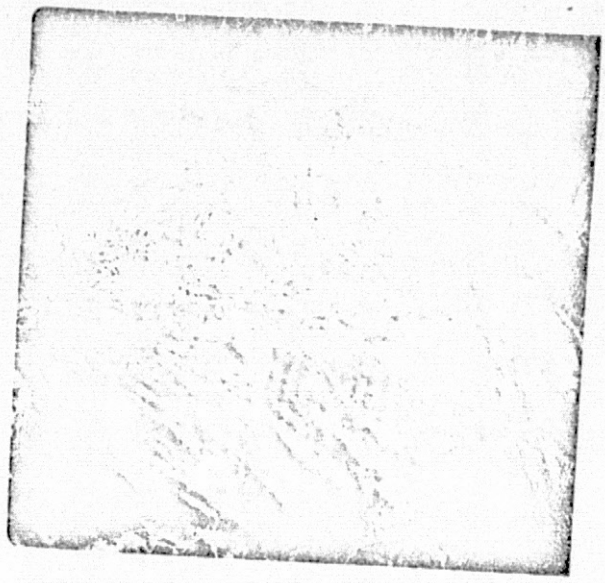

3. SL-4 photograph - NW part of Gulf of St. Lawrence
6 January 1974 - 139-3934

4. SL-4 photograph - NE part of Gulf of St. Lawrence
Straits of Belle Isle
11 January 1974 - 139-4072

5. SL-4 photograph – NE part of Gulf of St. Lawrence
Straits of Belle Isle
19 January 1974 – 141-4268

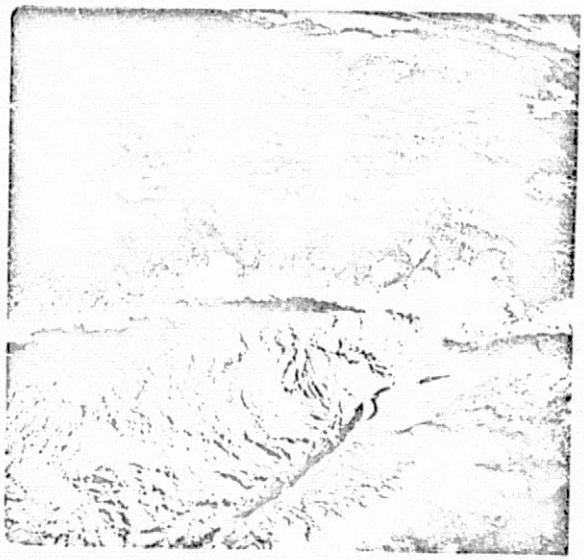

6. SL-4 photograph – NE part of Gulf of St. Lawrence
E part Straits of Belle Isle
20 January 1974 – 141-4326

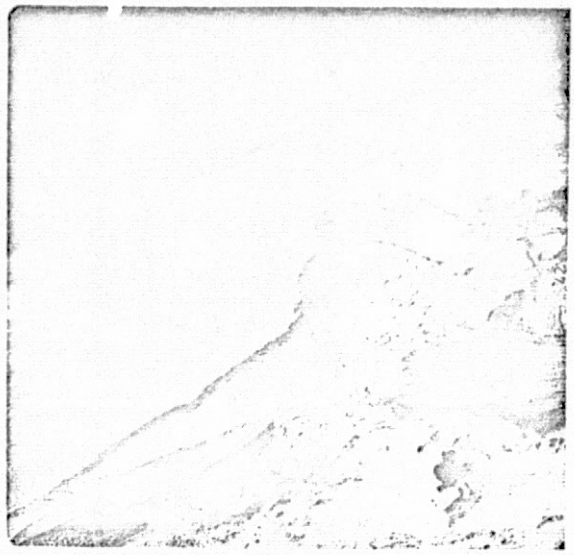

7. SL-4 photograph - Gulf of St. Lawrence
20 January 1974 - 141-4331

8. SL-4 photograph - W Gulf of St. Lawrence Gaspé Peninsula
18 January 1974 - 140-4215

9. SL-4 photograph - W Gulf of St. Lawrence Gaspé Peninsula
   20 January 1974 - 141-4321

10. SL-4 photograph - NW Gulf of St. Lawrence
    Anticosti Island
    18 January 1974 - 140-4216

11. SL-4 photograph - NW Gulf of St. Lawrence
Anticosti Island
20 January 1974 - 141-4327

12. SL-4 photograph - N Central Gulf of St. Lawrence
Anticosti Island
21 January 1974 - 141-4366

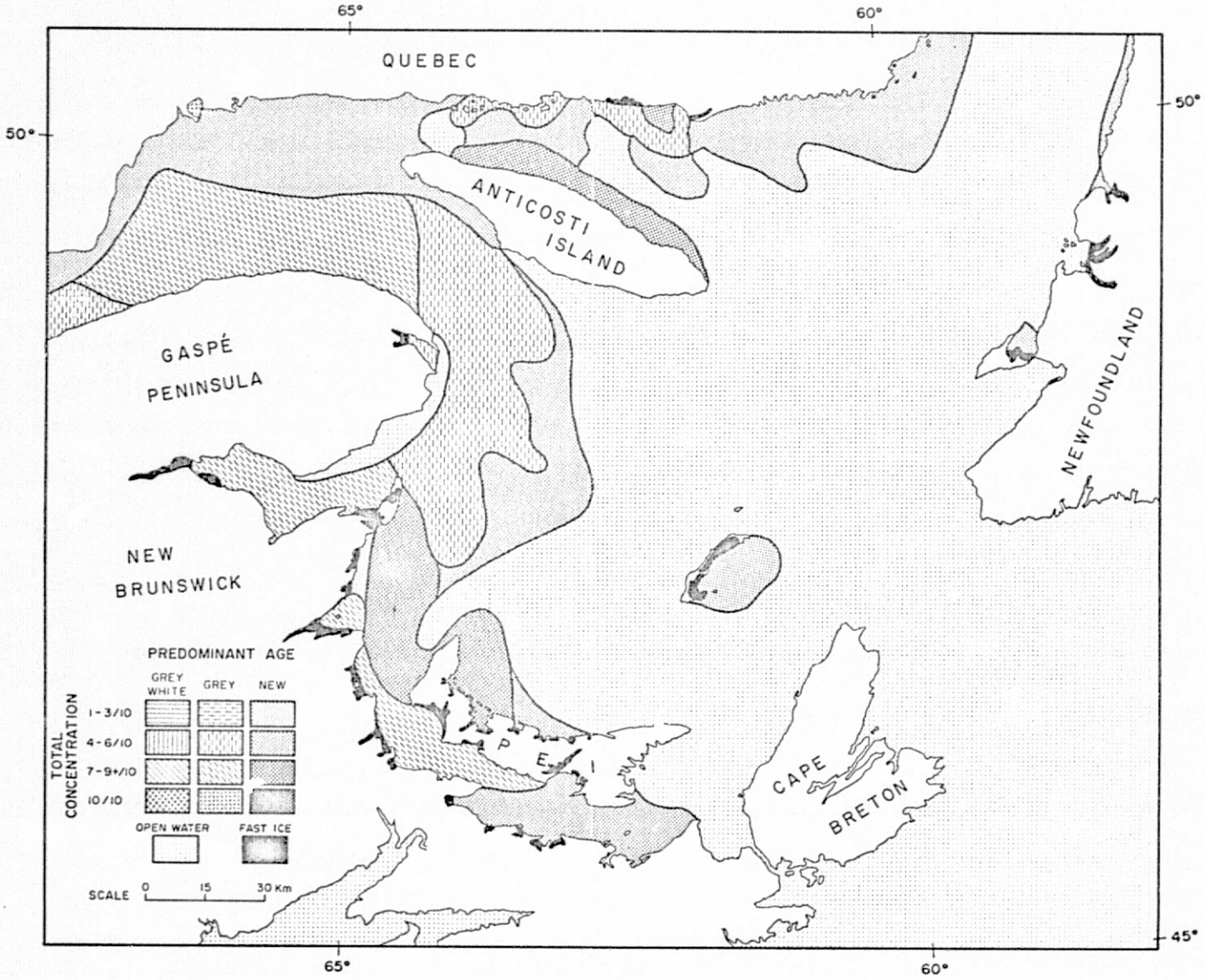

13. Ice Reconnaissance Map of Gulf of St. Lawrence, 8 January

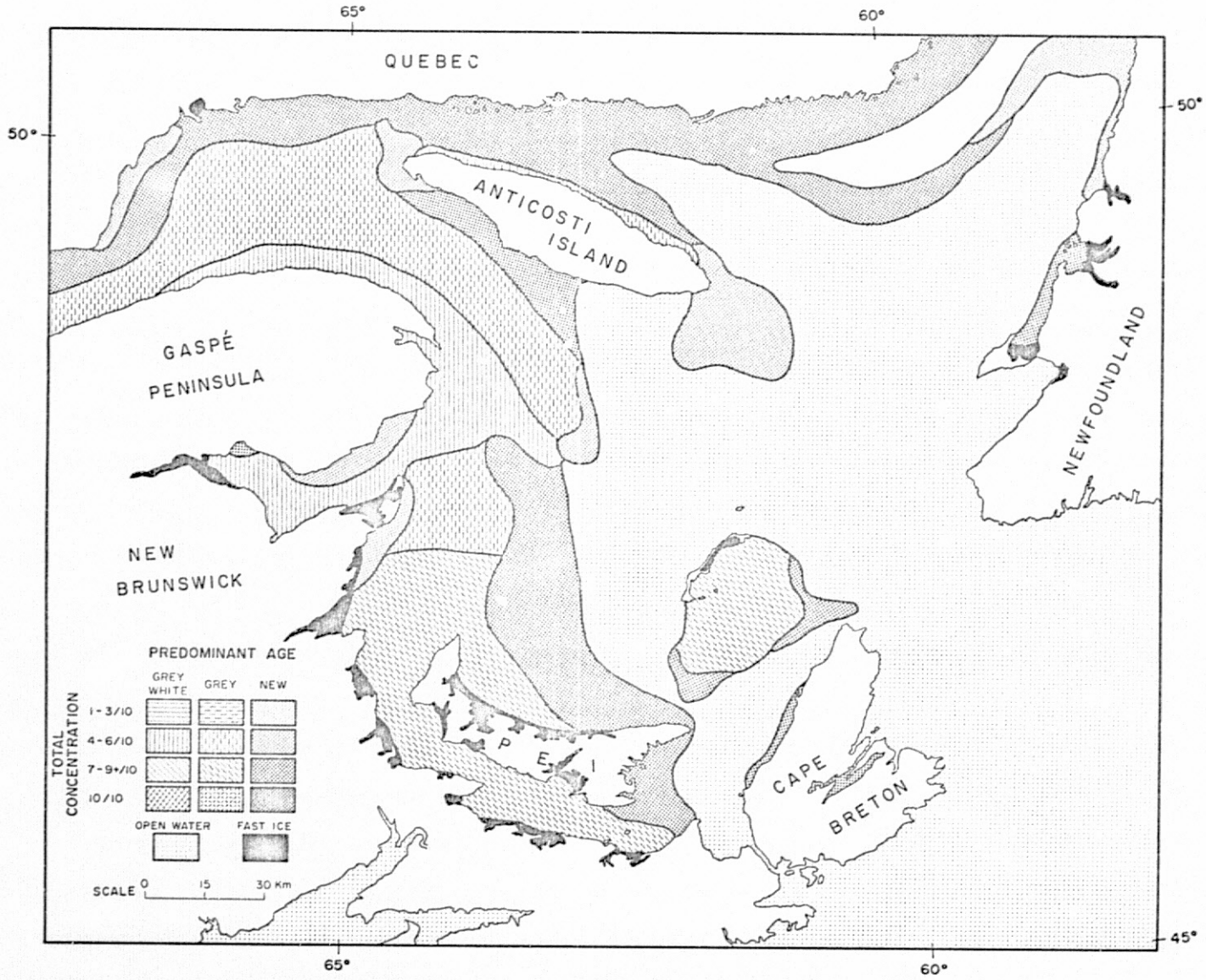

14. Ice Reconnaissance Map of Gulf of St. Lawrence, 13 January

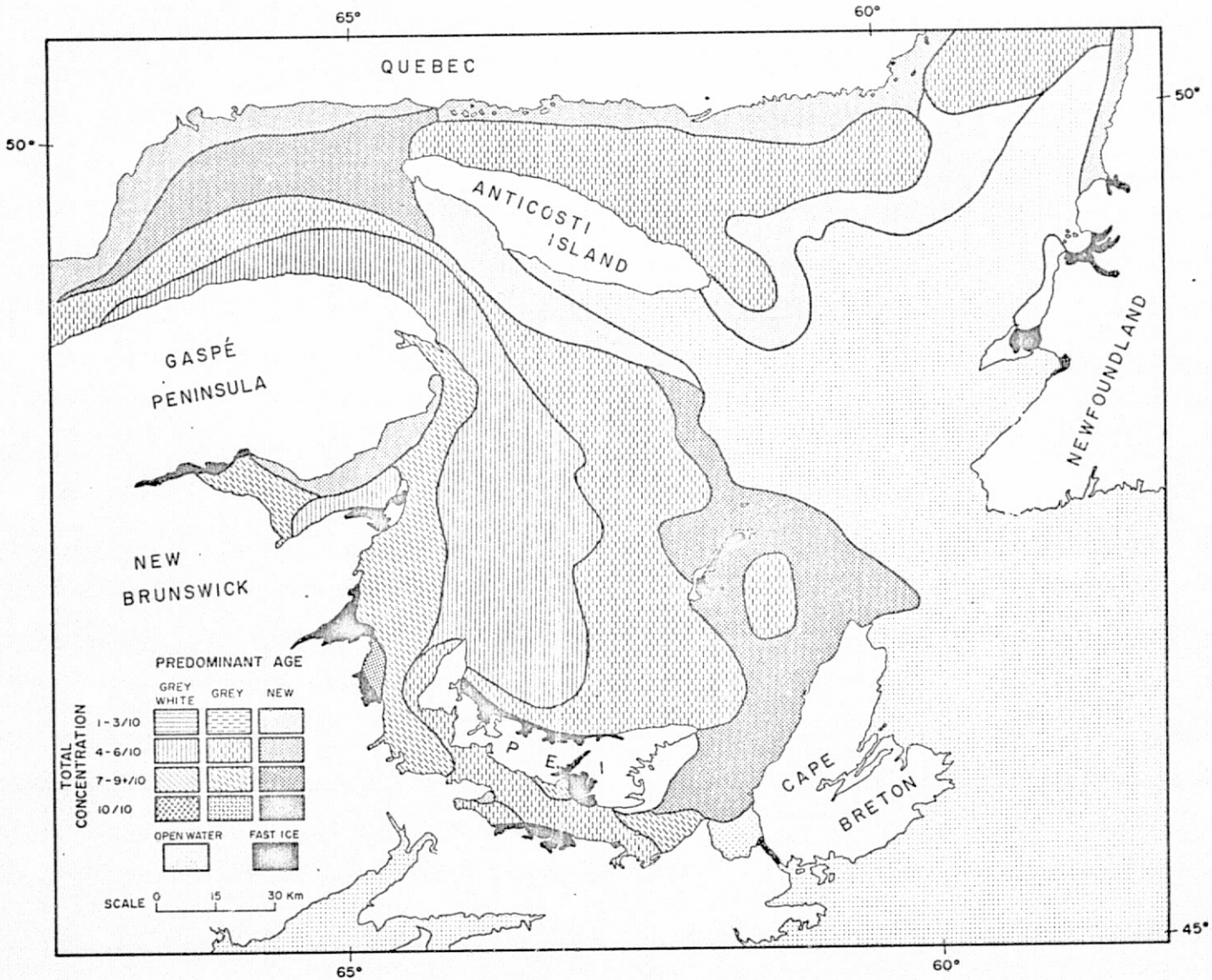

15. Ice Reconnaissance Map of Gulf of St. Lawrence, 18 January

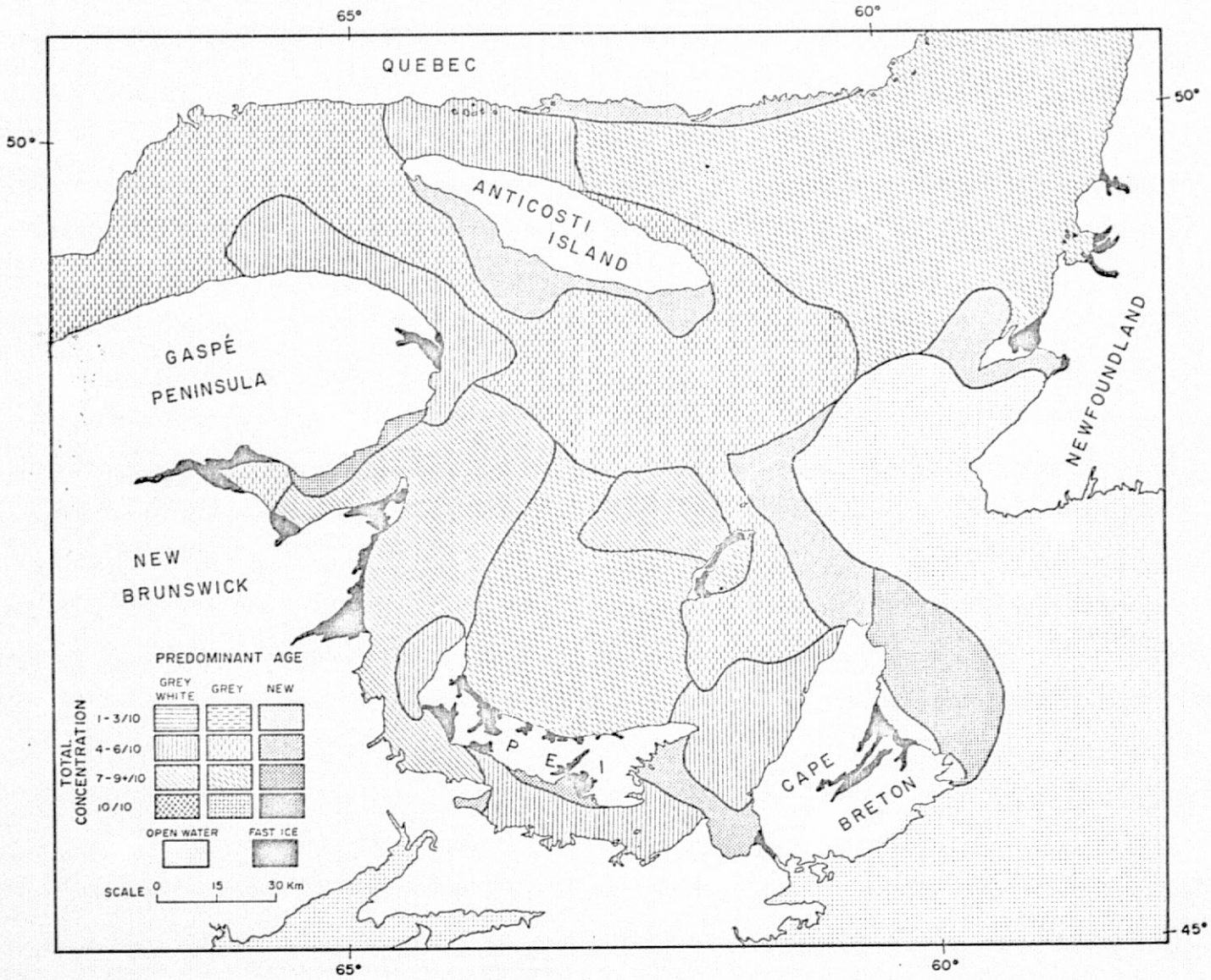

16. Ice Reconnaissance Map of Gulf of St. Lawrence, 22 January

Colour – 0.4 to 0.7 microns

Colour IR – 0.5 to 0.83 microns

IR – 0.6 to 0.7 microns

17. Three S190-A Multispectral Camera photographs of the Prince Edward Island area of the Gulf of St. Lawrence taken on 14 January 1974. The spectral ranges of each photograph are as follows:

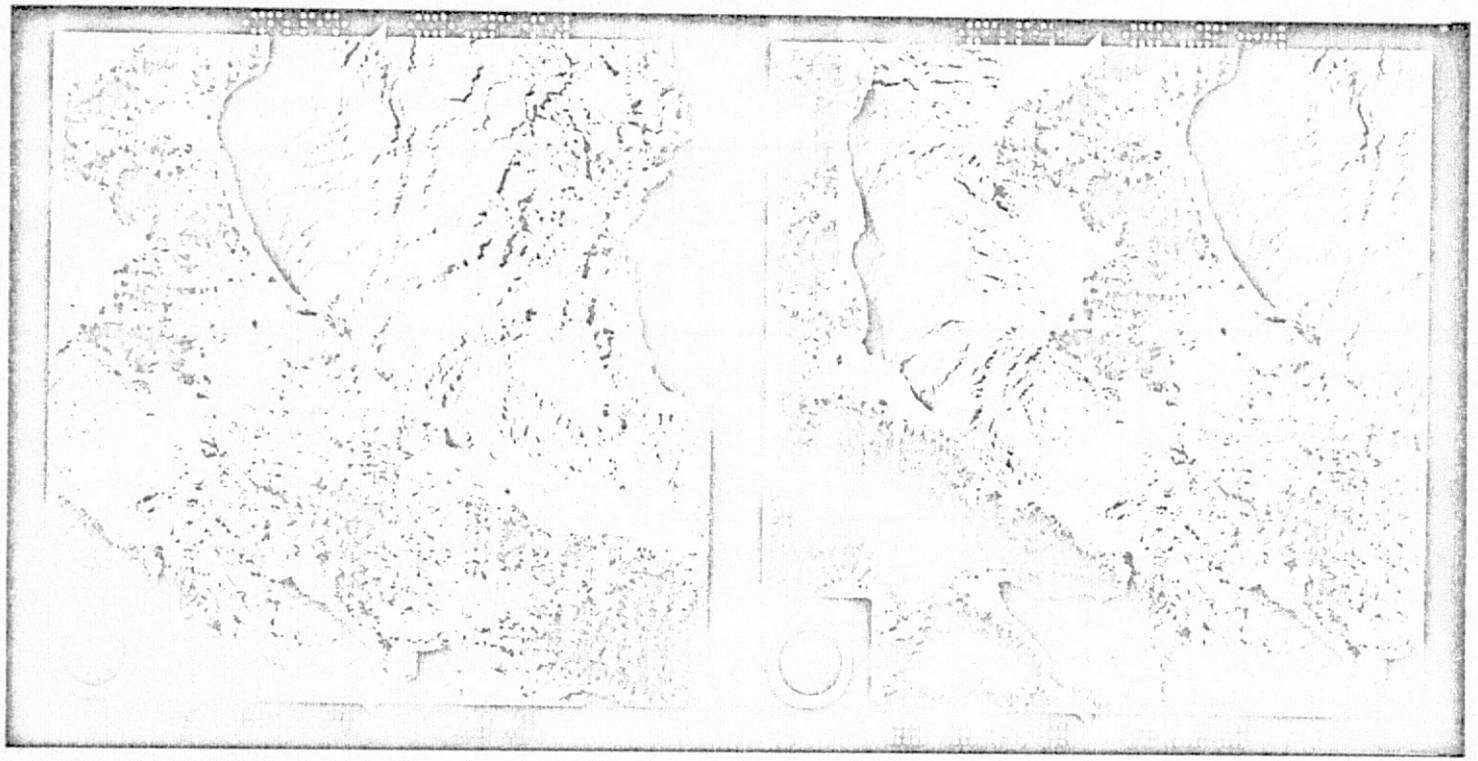

18. Two S190-B Earth Terrain Camera photographs of the Prince Edward Island area of the Gulf of St. Lawrence taken on 14 January 1974.

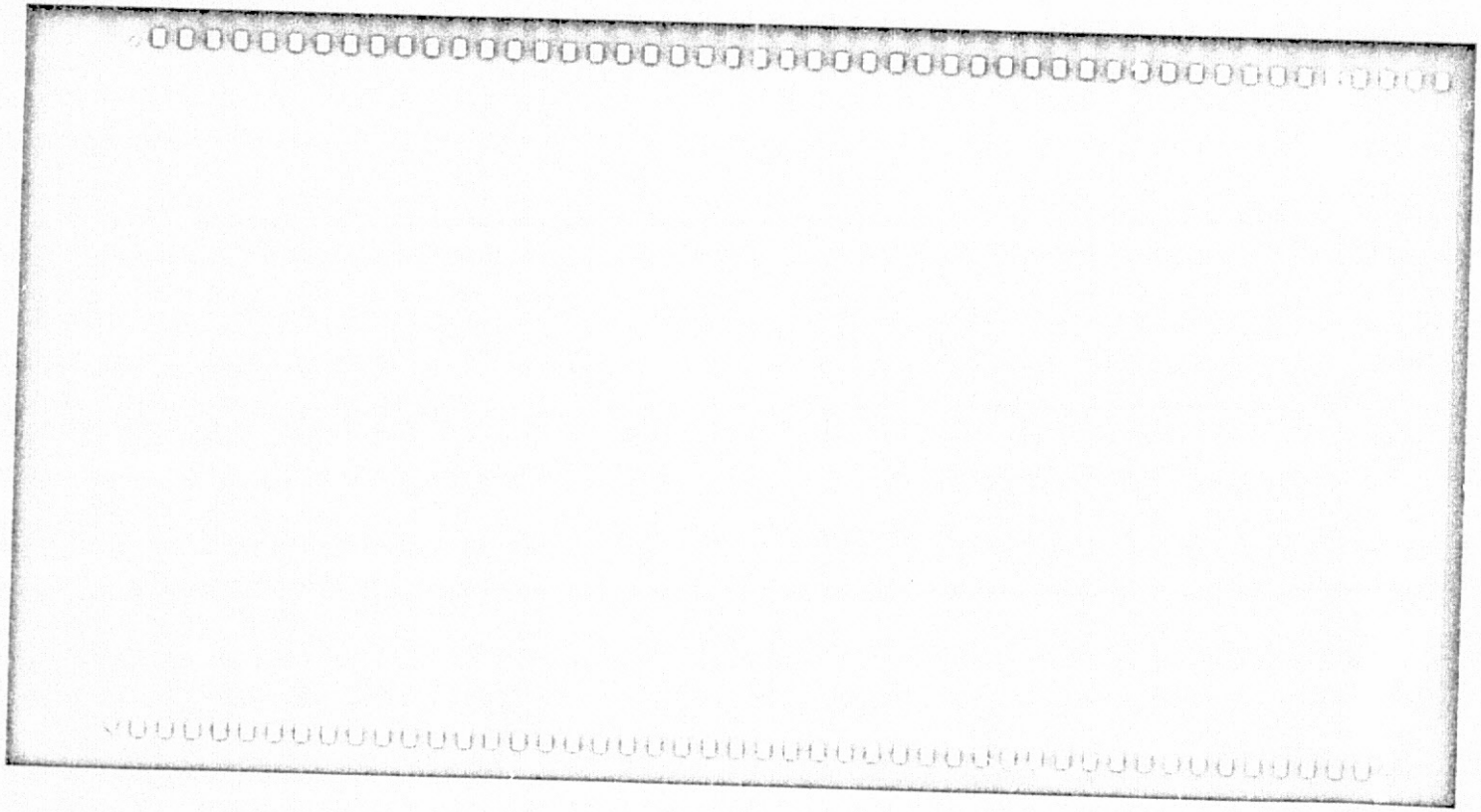

19. S192 infrared image of the Prince Edward Island area of the Gulf of St. Lawrence taken on 14 January 1974.

20. Two X-band side-looking airborne radar (SLAR) images of portions of the Gulf of St. Lawrence obtained by the Argus aircraft. (a) was taken on 13 January 1974 with a swath width of 50 km. (b) was taken on 18 January 1974 with a 25 km. swath width. The location of these SLAR runs is shown in Figure 1.

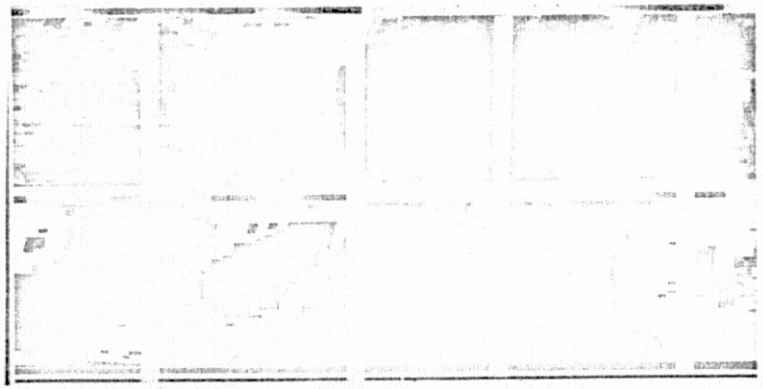

a) PMIS image

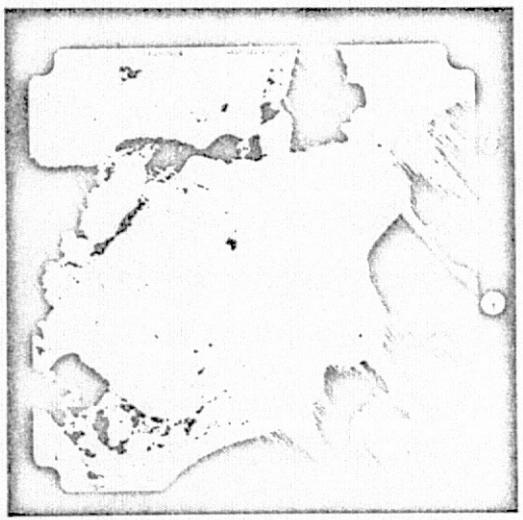

b) Ice plumes and frazil - grey ice mixture

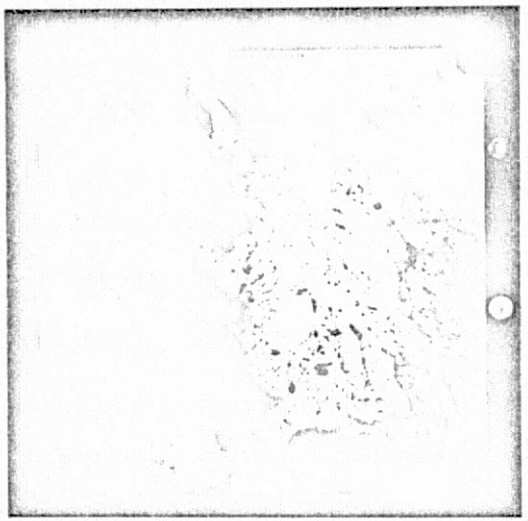

c) Grey-white ice

21. PMIS image and RC-8 photographs for Run I, Flight 19 on 16 January 1974 of the NASA NP-3A aircraft. The location of this run is shown in Figure 1.

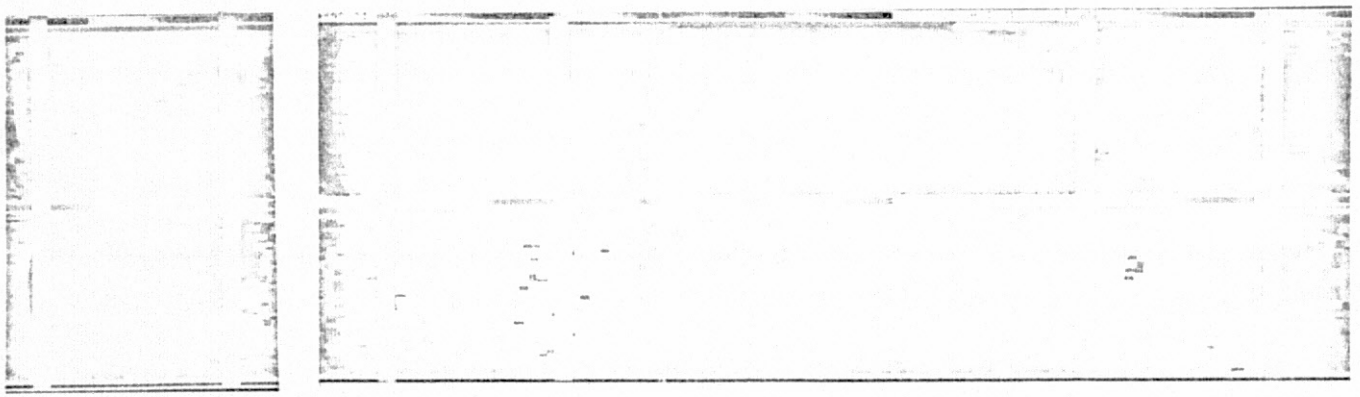

a) PMIS image

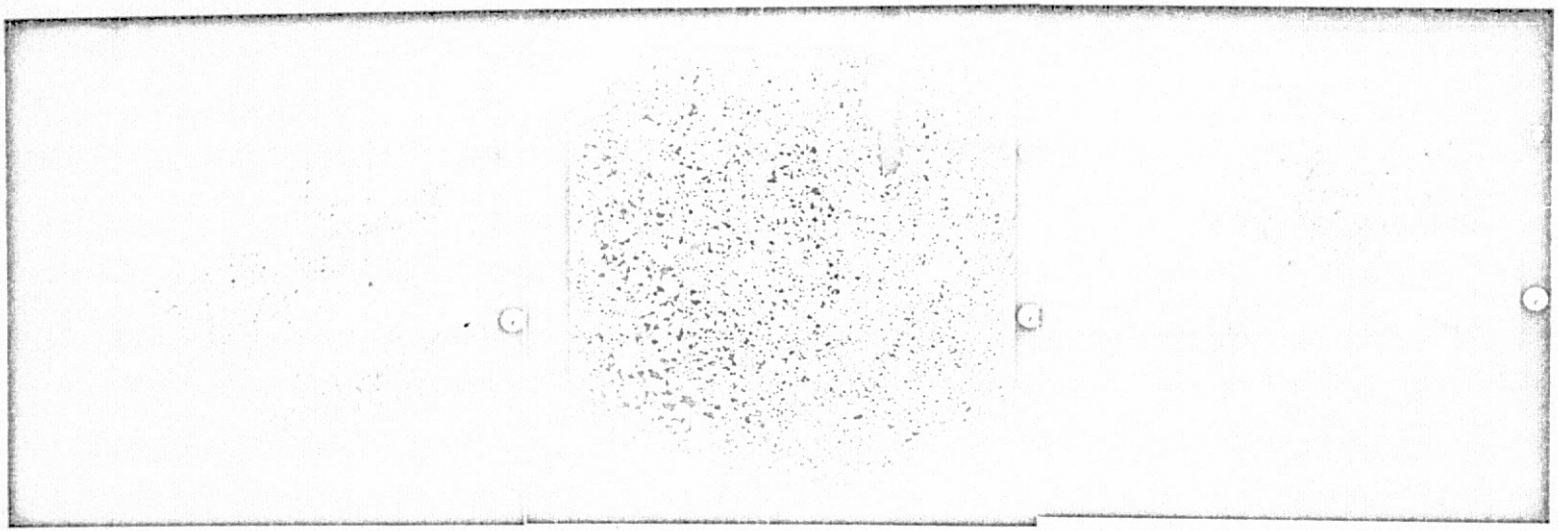

b) Consolidated pancake and grey-white ice

c) Pancake ice

d) Slush and frazil

22. PMIS image and RC-8 photographs for Run I, Flight 19 on 16 January 1974 of the NASA NP-3A aircraft. The location of this run is shown in Figure 1.

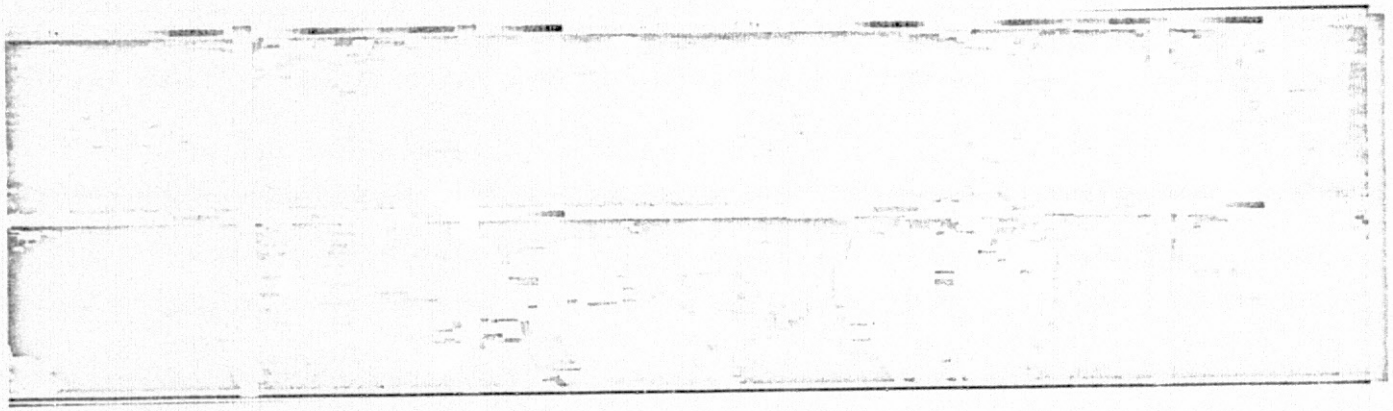

a) PMIS image

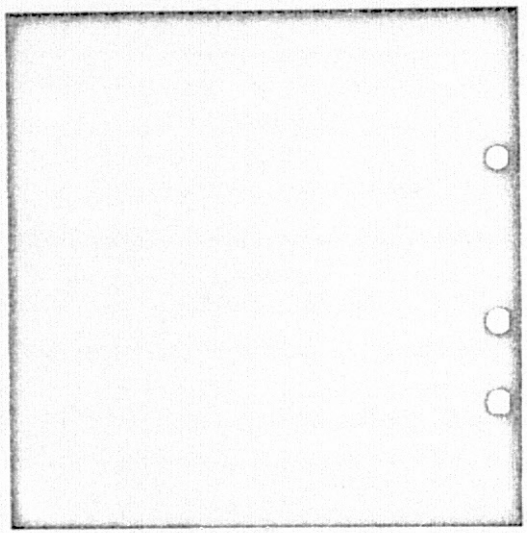

b) Nilas and grey ice

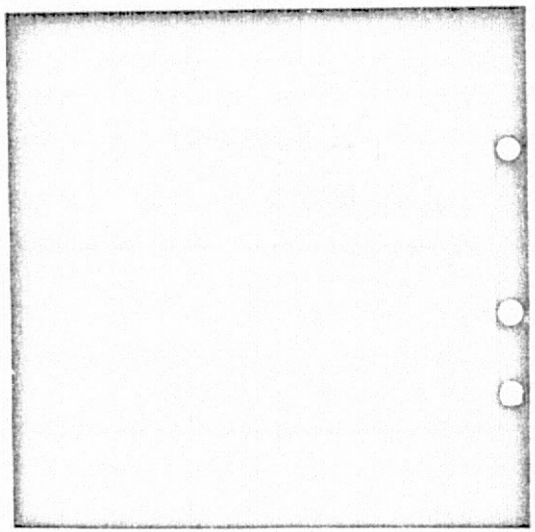

c) Grey-white and rafted ice

23. PMIS image and RC-8 photographs for Run 4, Flight 24 on 21 January 1974 of the NASA NP-3A aircraft. The location of this run is shown in Figure 1.

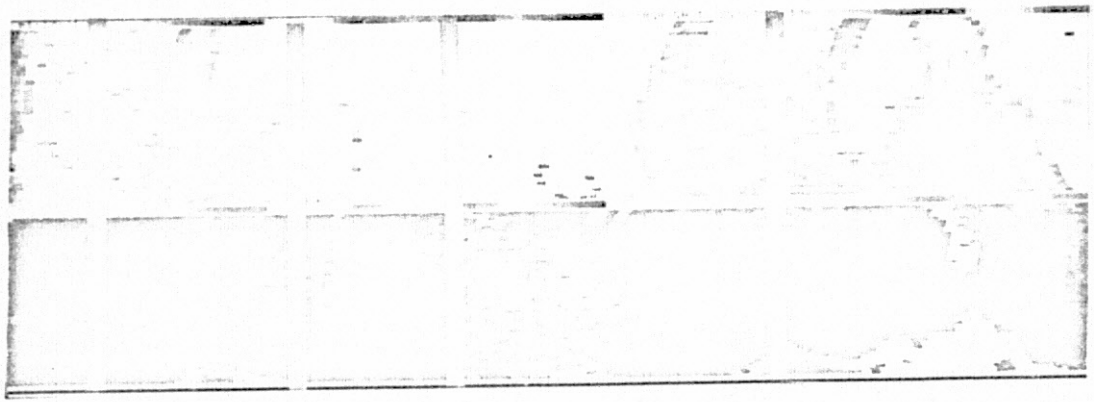

a) PMIS image

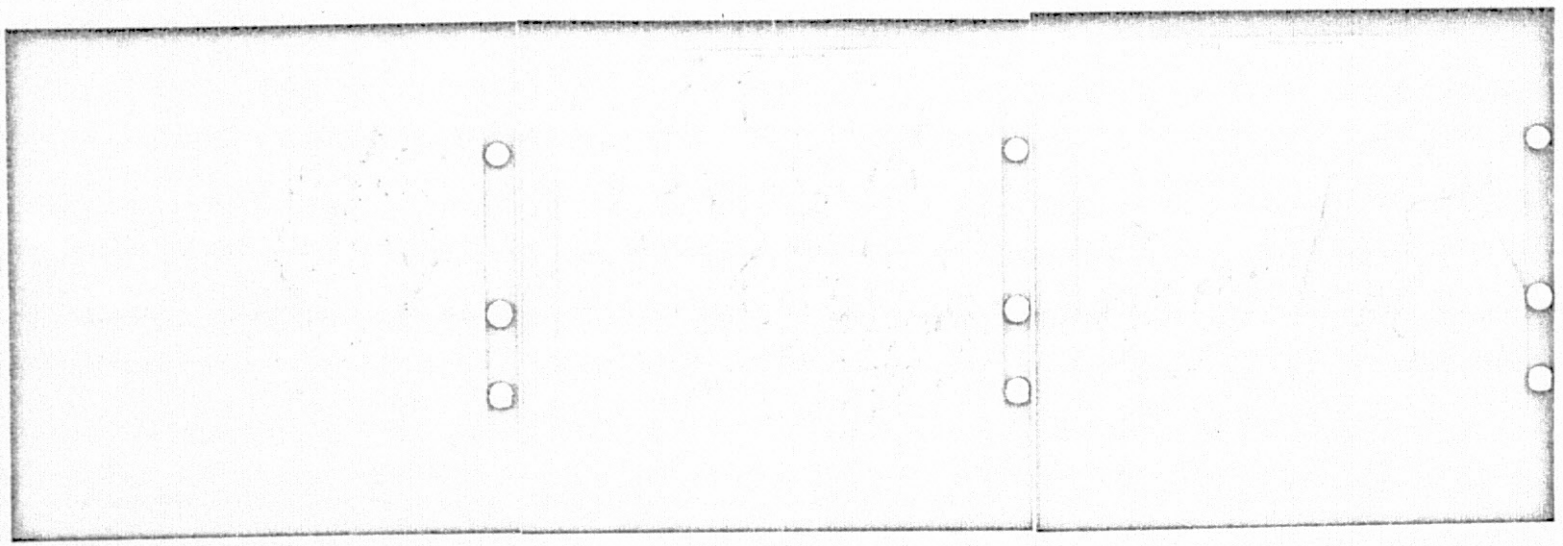

b) Nilas and grey ice

c) Grey ice

d) Grey ice and nilas

24. PMIS image and RC-8 photography for Run 3, Flight 24 on 21 January 1974 of the NASA NP-3A aircraft. The location of this run is shown in Figure 1.

a) PMIS image

b) Shorefast ice

c) Nilas

25. PMIS image and RC-8 photography for Run I, Flight 24 on 21 January 1974 of the NASA NP-3A aircraft. The location of this run is shown in Figure 1.

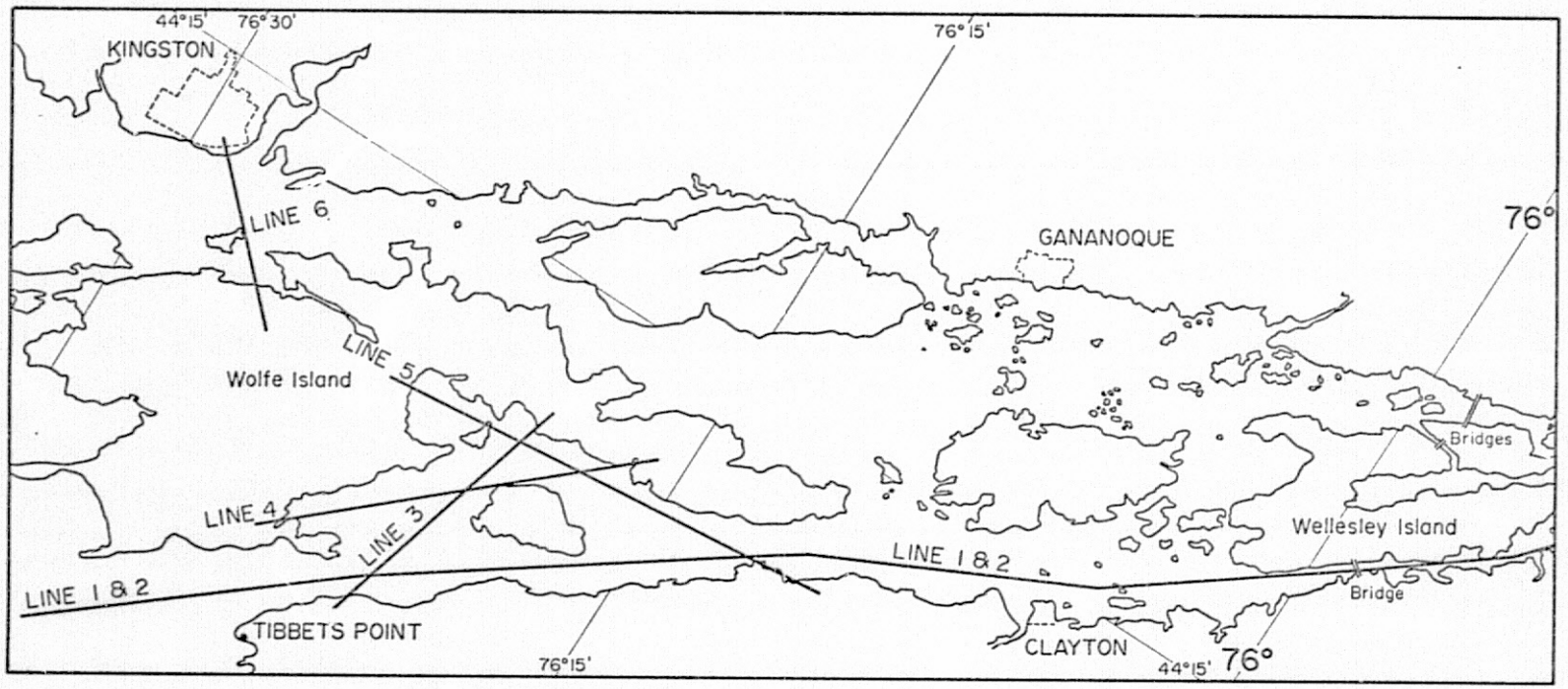

26. Map of St. Lawrence River-Thousand Islands area showing aircraft flight lines.

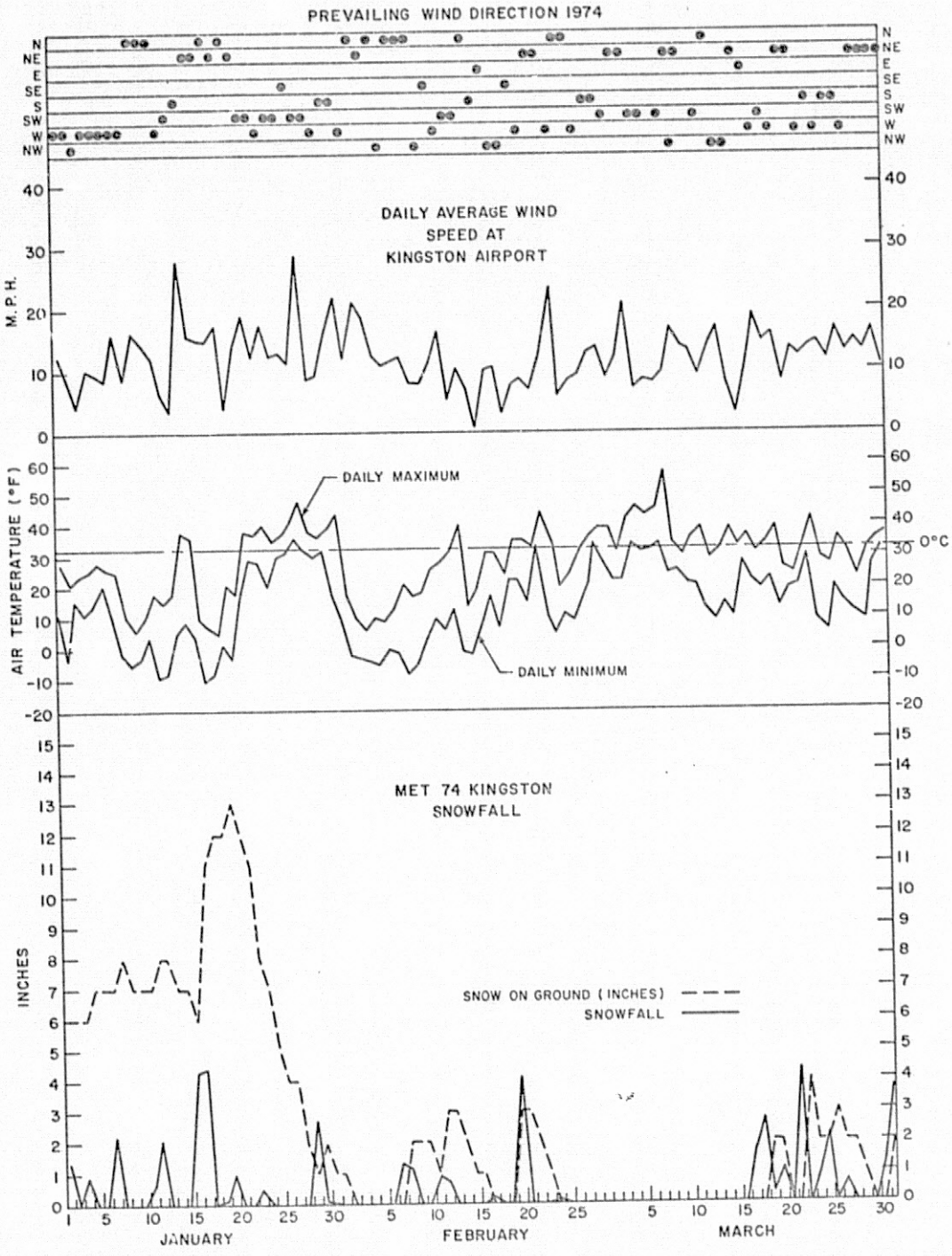

27. Meteorological data of the Thousand Islands area showing windspeed and direction, daily maximum and minimum air temperatures and the amount of snow precipitation.

A

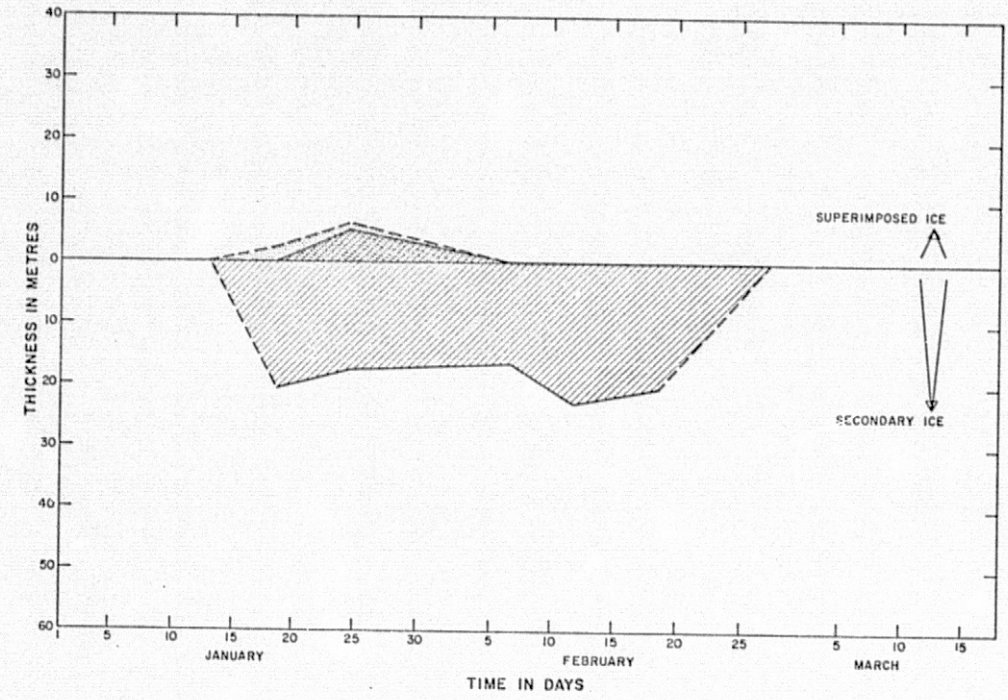

B

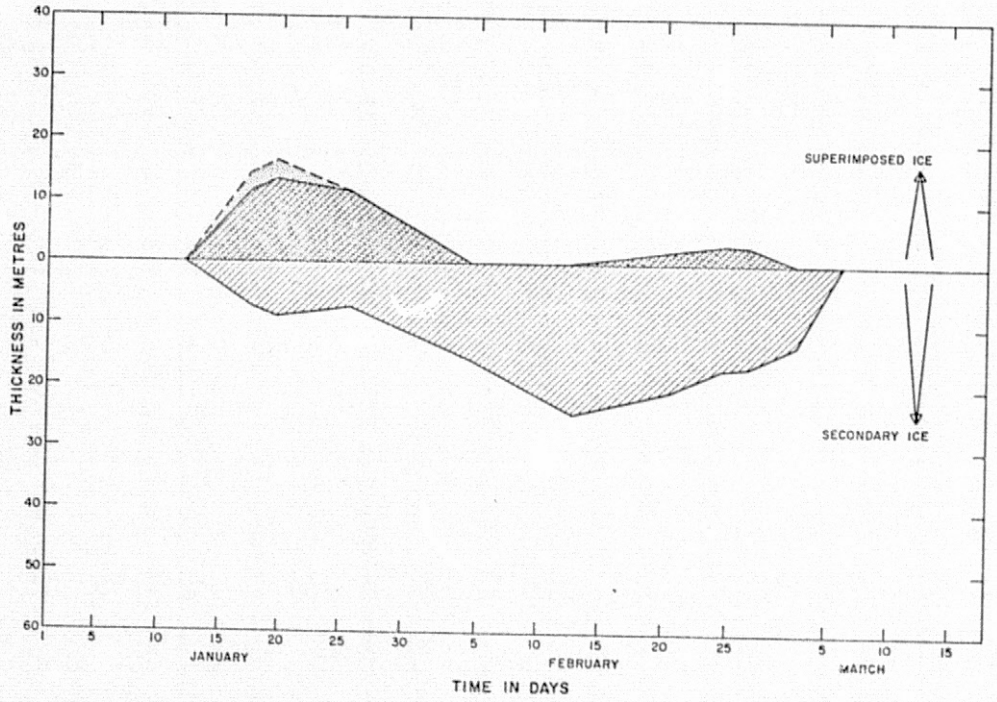

28. Ice thickness station profiles showing the thickness due to secondary and superimposed ice. A) Station H-3 9.65 km; B) Station 6 78.8 km; C) Station 12 99.7 km and D) Station 17 102.2 km from Prescott-Ogdensburg.

C

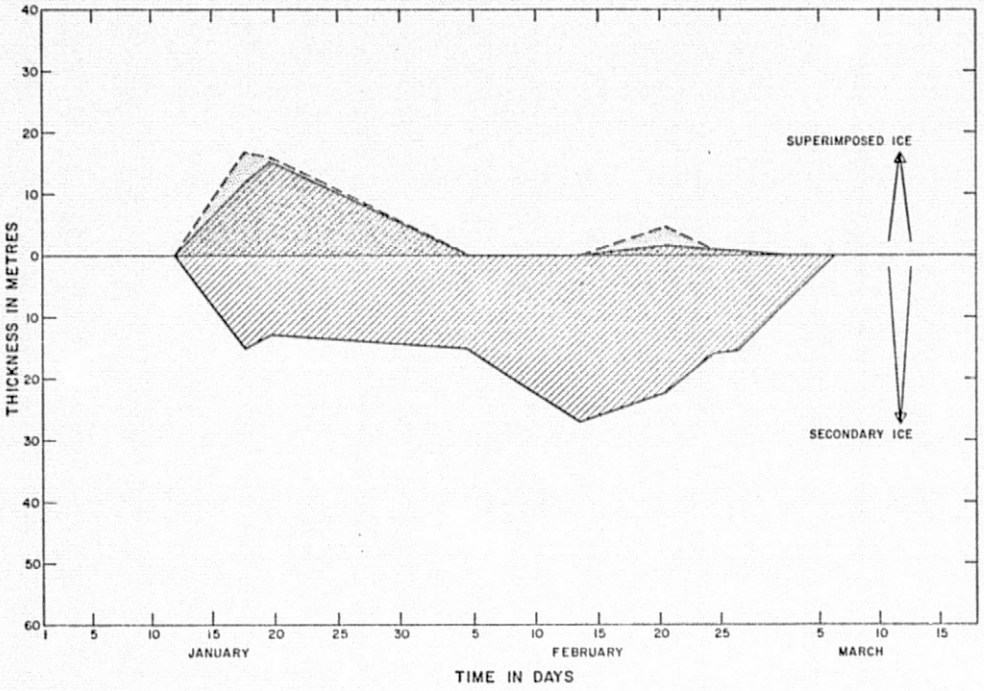
THICKNESS IN METRES
SUPERIMPOSED ICE
SECONDARY ICE
JANUARY
FEBRUARY
MARCH
TIME IN DAYS

D

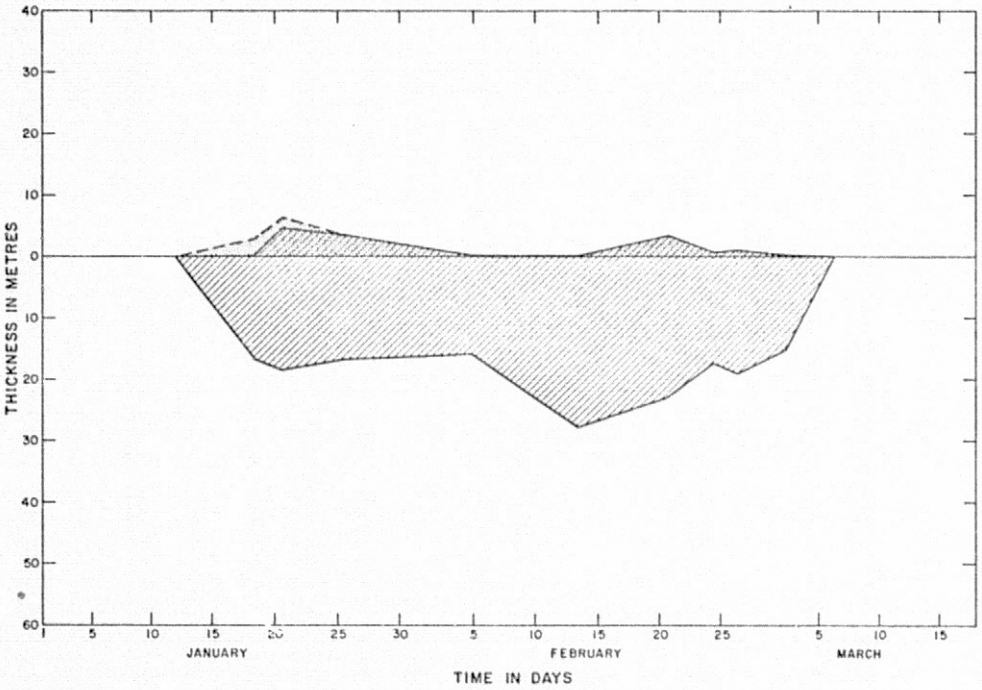
THICKNESS IN METRES
JANUARY
FEBRUARY
MARCH
TIME IN DAYS

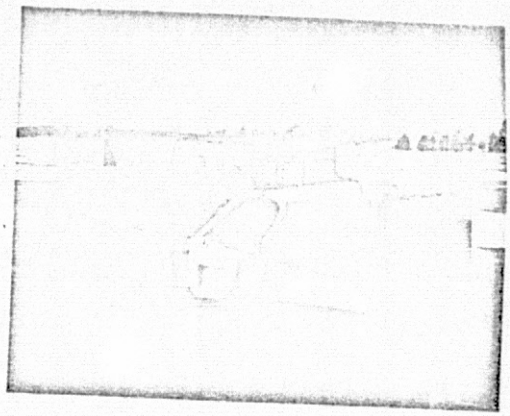

29. Part A shows the air-cushion vehicle on which the hour of the X-band impulse radar is visible. The generator for the power supply is mounted on the opposite side of the antenna on top of the frame. The ACV is sitting on top of black ice (secondary ice) surrounded by patches of white superimposed ice (snow ice) on top of secondary ice.

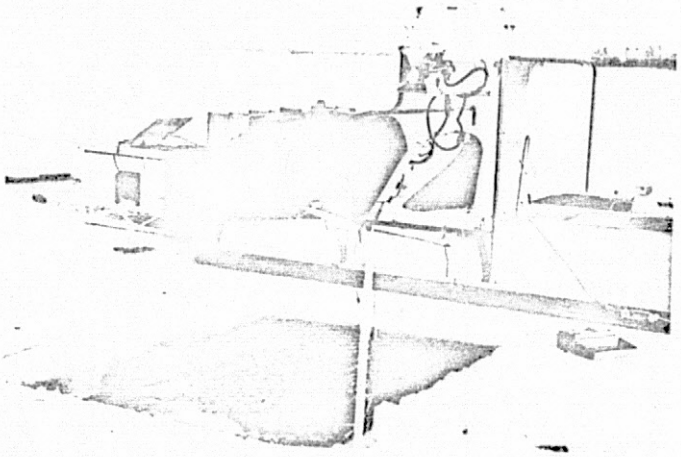

Part B shows the ACV with Aerojet Electrosystems 37 GHz passive microwave radiometer. In this particular setup the brightness temperature was determined as a function of ice thickness (during the growth of secondary ice).

30. Photomosaic and PMIS imagery of part of the St. Lawrence River - Morristown to Ogdensburg. This data was obtained along flight line 1 at an altitude of 2225 m on February 4, 1974.

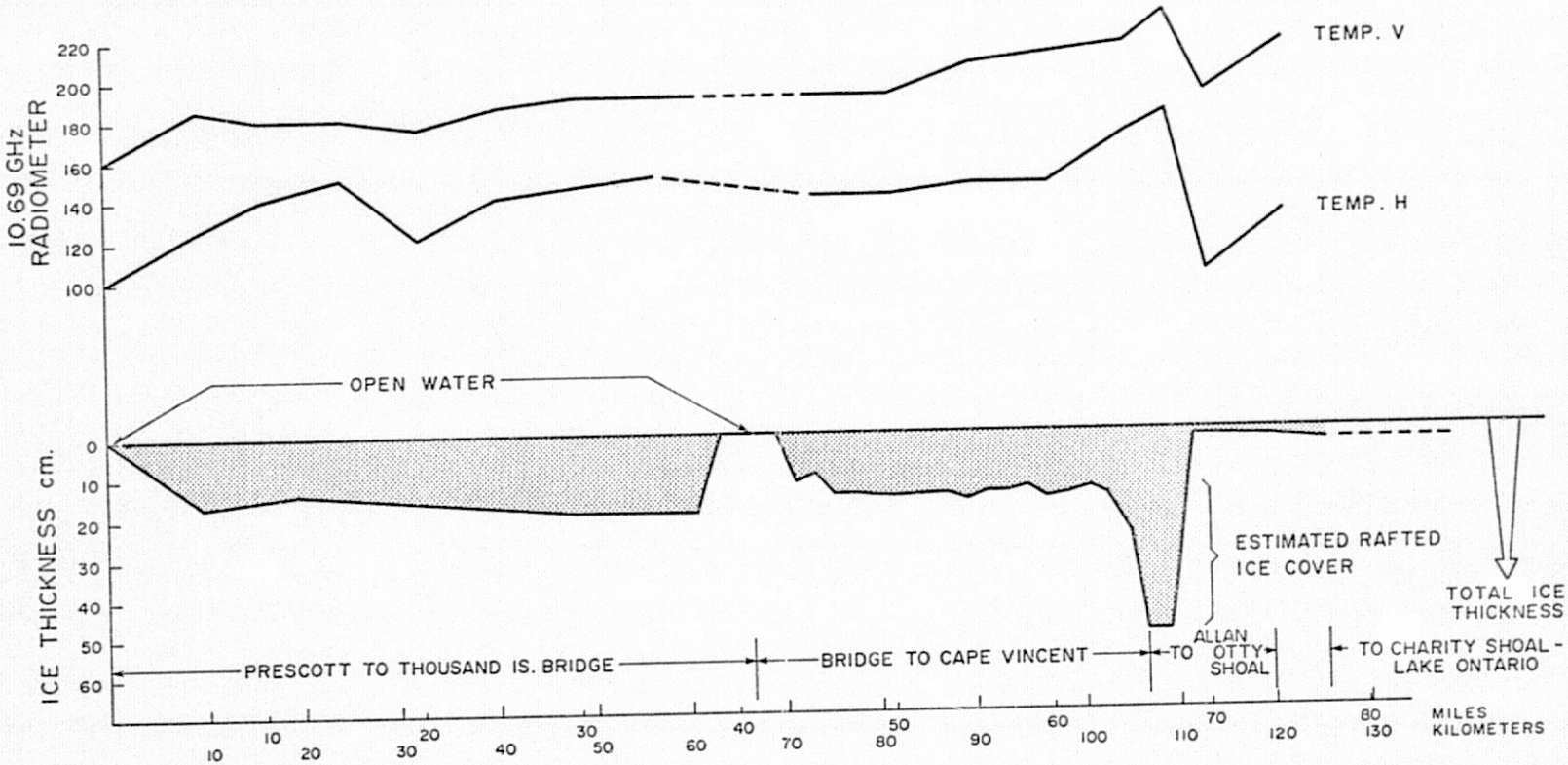

3 Ice thickness and PMIS brightness temperature profile along flight line 1.

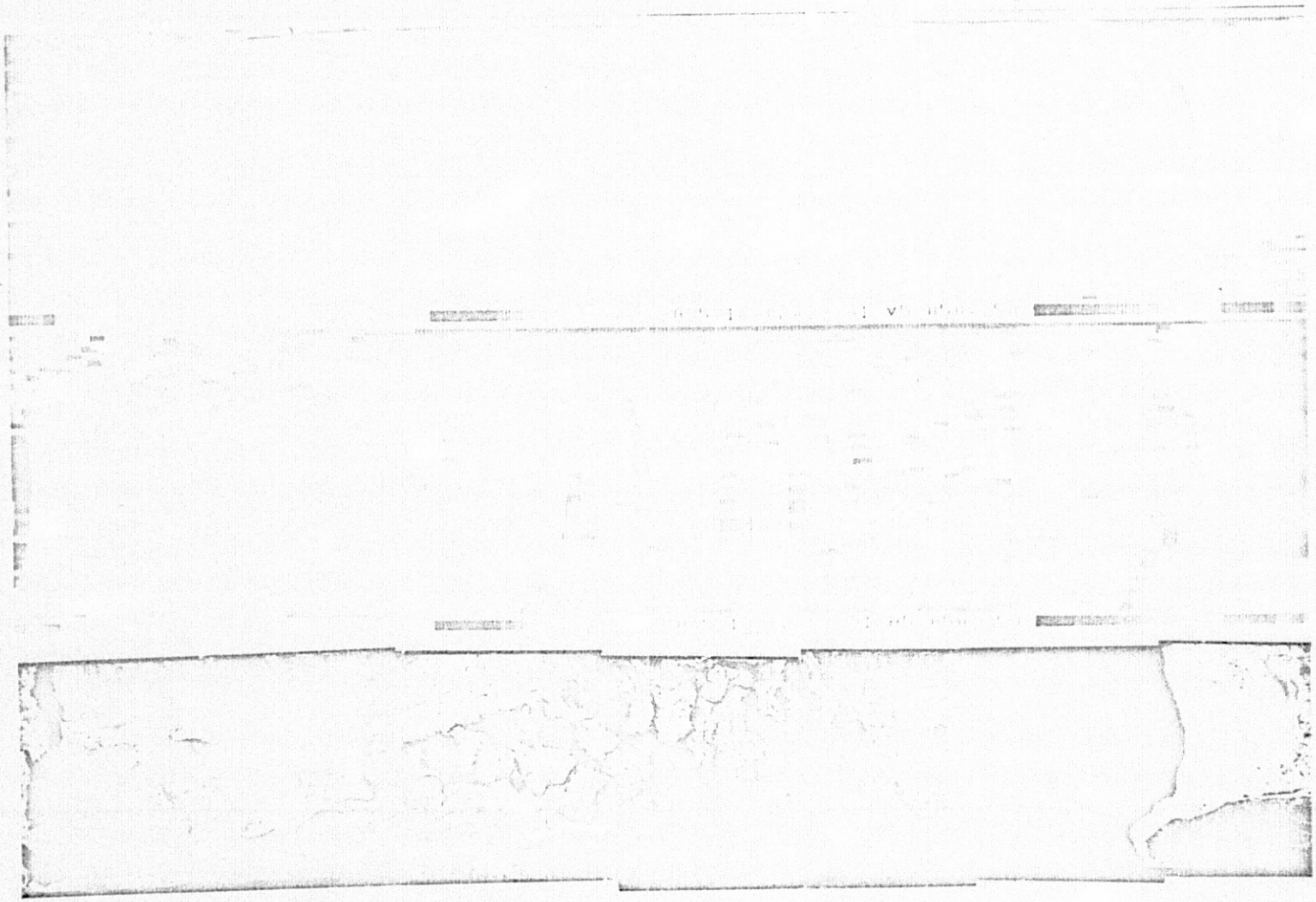

32. Photomosaic and PMIS imagery of Tibbetts Point and Lake Ontario along the beginning of line 1, taken at an altitude of 700 m.

33. Photomosaic and PMIS imagery along line 4 north of Carleton Island, taken at an altitude of 700 m.

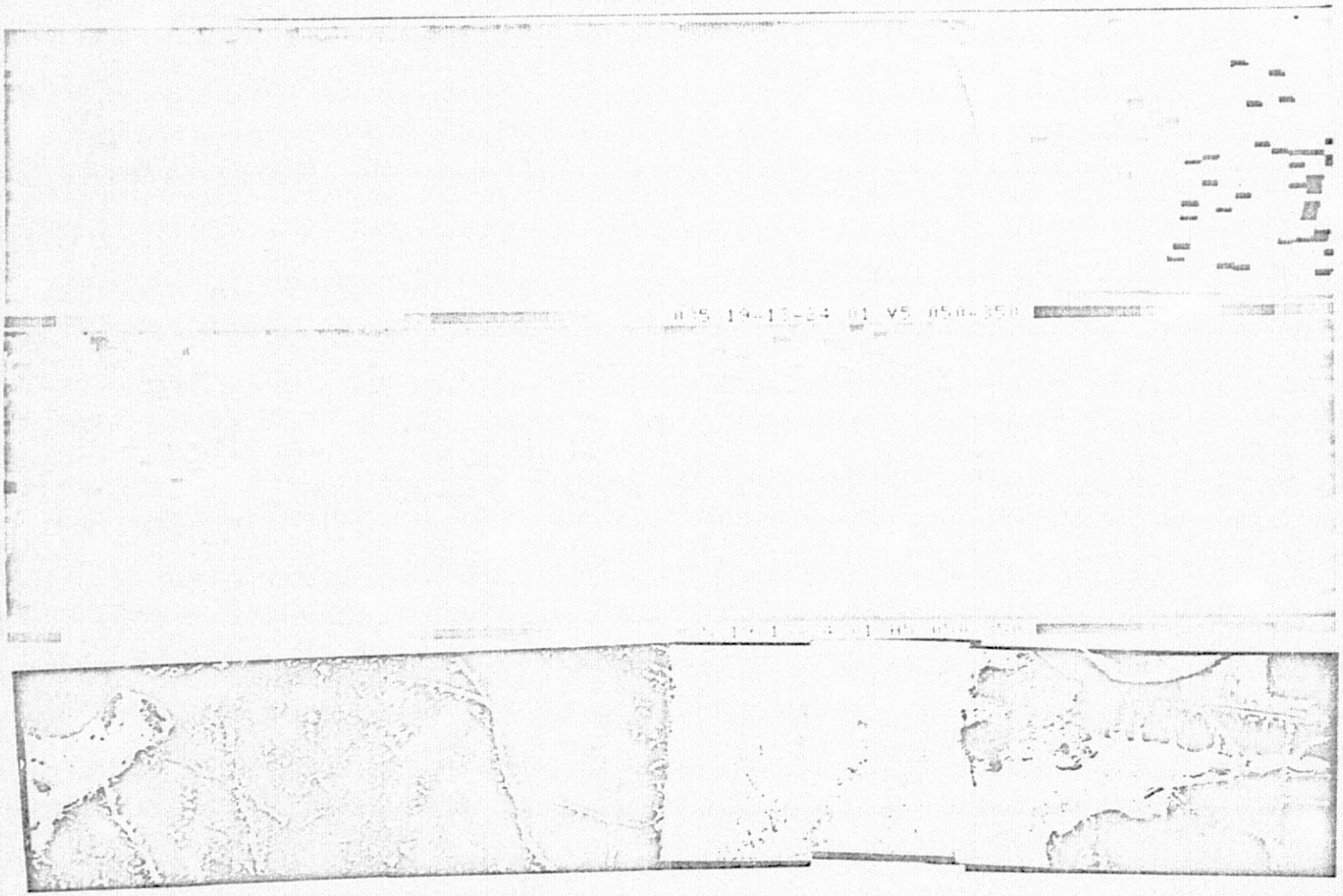

34. Photomosaic and PMIS imagery at the end of line 4 over Button Bay taken at an altitude of 700 m.

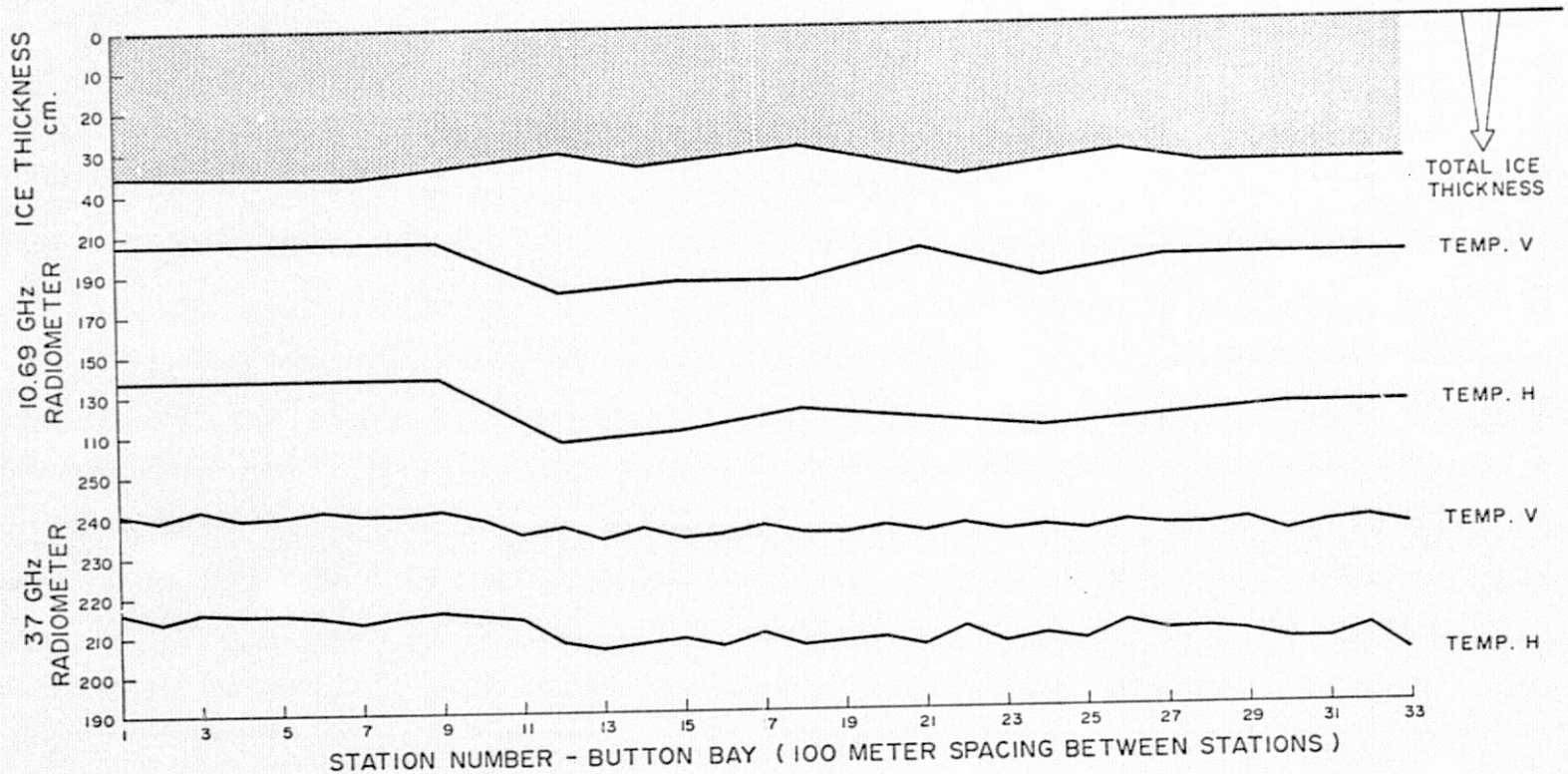

35. Ice thickness and brightness temperature profiles for 10.69 GHz and 37 GHz. PMIS and Aerojet passive microwave radiometers respectively. This area corresponds to the shorefast and black ice area in Figure 34.

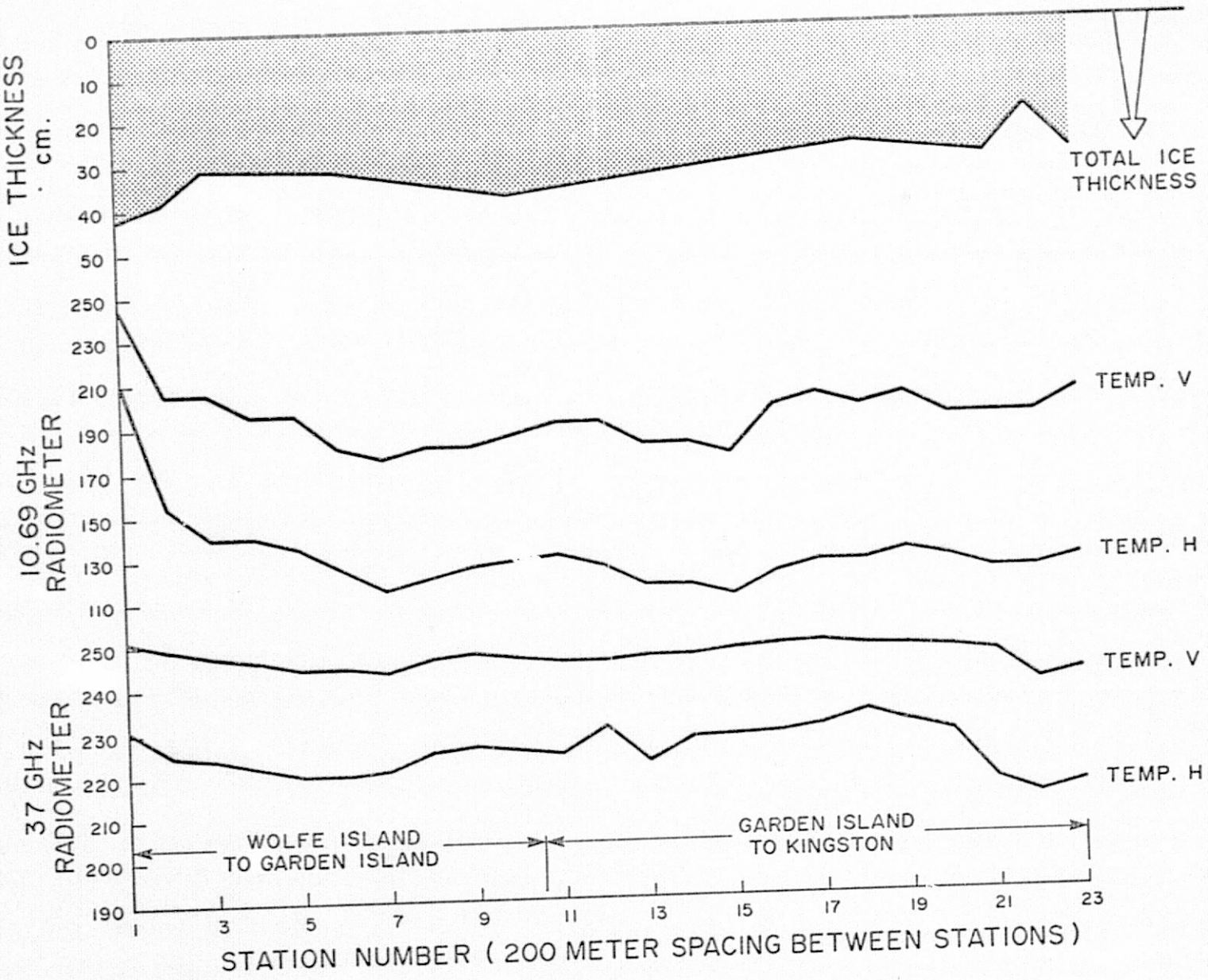

36. Ice thickness and brightness temperature profiles for 10.69 GHz and 37 GHz PMIS and Aerojet passive microwave radiometer respectively. These profile correspond to flight line 6.

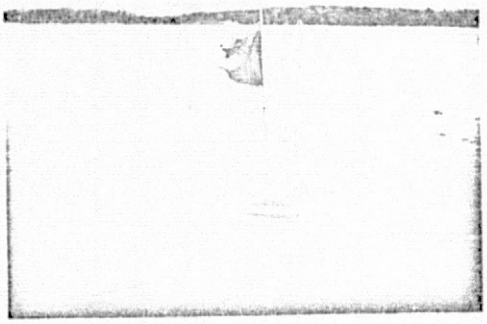

a) Black ice

b) Refrozen ice floe field

c) Ridge at Lake Ontario - St. Lawrence River interface.

37. Surface photographs of some distinct ice conditions